IDENTIFICATION OF SEVERAL ENERGY TRANSFER PATHWAYS IN THE LIGHT-HARVESTING COMPLEX II OF GREEN PLANTS USING CURRENT STRUCTURAL AND SPECTROSCOPIC INFORMATION

A THESIS SUBMITTED TO
THE GRADUATE SCHOOL OF NATURAL AND APPLIED SCIENCES
OF
THE MIDDLE EAST TECHNICAL UNIVERSITY

BY

SEVGİ ÖZDEMİR

IN PARTIAL FULFILLMENT OF THE REQUIREMENTS FOR THE DEGREE OF

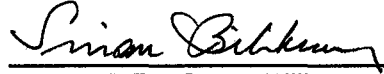MASTER OF SCIENCE

IN

THE DEPARTMENT OF PHYSICS

JANUARY 1997

Approval of the Graduate School of Natural and Applied Sciences

Prof. Dr. Tayfur Öztürk
Director

I certify that this thesis satisfies all the requirements as a thesis for the degree of Master of Science.

Prof. Dr. Sinan Bilikmen
Head of Department

This is to certify that we have read is thesis and in our opinion it is fully adequate, in scope and quality, as a thesis for the degree of Master of Science.

Assoc. Prof. Dr. Demet Gülen
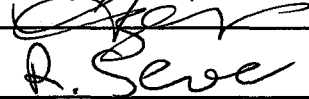Supervisor

Examining Committee Members

Prof. Dr. Ramazan Aydın

Prof. Dr. İnci Eroğlu

Prof. Dr. Ay Melek Özer

Prof. Dr. Ramazan Sever

Assoc. Prof. Dr. Demet Gülen

ABSTRACT

IDENTIFICATION OF SEVERAL ENERGY TRANSFER PATHWAYS
IN THE LIGHT-HARVESTING COMPLEX II OF GREEN PLANTS
USING CURRENT STRUCTURAL AND SPECTROSCOPIC INFORMATION

Özdemir, Sevgi

M.S., Department of Physics

Supervisor: Assoc. Prof. Dr. Demet Gülen

January 1997, 56 pages.

A set of procedures to run numerical experiments to investigate the excitation dynamics (energy transfer processes) in a structurally resolved network of molecules has been developed. The procedures have been used to simulate the energy transfer processes in the Light-Harvesting Complex II (LHCII) of green plants. Energy transfer between a pair of molecules (chlorophylls) of the complex has been modeled by the Förster mechanism and time evolution of the excitations has been evaluated in the Pauli master equation formalism. The aim of the simulations has been to correlate some of the processes observed in the sub-picosecond time-resolved measurements with the current LHCII structural model. Several possibilities for the energy transfer pathways among the chlorophylls of the LHCII complex have been identified.

Key Words: Photosynthesis, Light-Harvesting Complex, Energy Transfer, Förster Mechanism, Pauli Master Equation, Femtosecond Spectroscopy.

ÖZ

YEŞİL BİTKİLERİN IŞIK-DERLEYİCİ II SİSTEMİNDE ÇEŞİTLİ ENERJİ TRANSFER SÜREÇLERİNİN YAPISAL VE SPEKTROSKOPİK BİLGİLER ÇERÇEVESİNDE BELİRLENMESİ

Özdemir, Sevgi

Yüksek Lisans, Fizik Bölümü

Tez Yöneticisi: Assoc. Prof. Dr. Demet Gülen

Ocak 1997, 56 sayfa.

Yapısal olarak çözümlenmiş molekül ağlarında uyarılmış durumların dinamiğini (enerji transfer süreçlerini) araştırabilmek amacıyla bir dizi nümerik prosedür geliştirildi. Geliştirilen prosedürler, yeşil bitkilerin Işık-Derleyici Sistem' inde (LHCII) enerji transfer süreçlerinin simülasyonu için kullanıldı. Sistemin molekülleri (klorofil) arasındaki enerji transfer süreçleri Förster mekanizması ile modellendi ve uyarılmış durumların zaman içinde değişimi Pauli master denklemi çerçevesinde değerlendirildi. Simülasyonların amacı deneylerde gözlemlenen birtakım hızlı (femtosaniye) süreçlerin LHCII' nin yapısal modeliyle korelasyonu olarak özetlenebilir. LHCII sisteminin klorofilleri arasındaki olası enerji transfer kanalları belirlendi.

Anahtar Kelimeler: Fotosentez, Işık-Derleyici Sistem, Enerji Transferi, Förster Mekanizması, Pauli Master Denklemi, Femtosaniye Spektroskopisi.

ACKNOWLEDGMENTS

TABLE OF CONTENTS

LIST OF TABLES

LIST OF FIGURES

CHAPTER 1

INTRODUCTION

Plants, algae and certain bacteria convert solar energy into storable chemical energy by photosynthesis. This process can be divided into two main types of reactions. The light reactions are based on the principle of the light absorption coupled with electronic energy migration and trapping. This reaction leads to production of molecular oxygen and high-energy chemical products. These compounds are adenosine triphosphate (ATP) and reduced nicotinamide adenine dinucleotide phosphate ($NADPH_2$). During the dark reactions these high-energy chemical products are used to reduce carbon dioxide to carbohydrate. Thus carbohydrate is the end product of photosynthesis and is the stabilized energy storage product [1].

In green plants and most algea, two primary processes of photosynthesis are the excitation energy transfer in light-harvesting complexes, LHCs, and the electron transfer in reaction centers, RCs. These processes take place in a highly organized LHC/RC complexes embedded in the photosynthetic membrane.

Upon absorption of solar energy by chlorophylls (Chls) in LHC, electronic excitations (excited states) are created. A chain of excitation energy transfers are carried out in LHC and energy is eventually transferred to RC. This energy initiates the charge separation process in the RC, and a potential difference across the photosynthetic membrane is created. This potential gradient provides the energy necessary to drive further chemical reactions. Excitation transfer energy in LHC and charge separation in RC are very fast and efficient.

The main questions asked on these primary processes are:

- What is the structure of the LHC/RC complex ?

and

- What are the mechanisms that cause these complexes to carry out their functions?

Recent advances in ultrafast spectroscopy, structure determination, and genetic engineering are leading to a better understanding of the structure-function relationship. We refer to several review articles for further information [1-6].

In this thesis our main concern has been on the light harvesting physics of the LHCII. This Chl *a/b* protein complex is the main LHC in green plants. A large part of the LHCII structure has recently been modeled by Kühlbrandt and co-workers [7].

Our objective has been to identify the major energy transfer pathways between the Chls of the LHCII within the current state of structural understanding provided by Kühlbrandt and co-workers. [7] and Gülen and

2

co-workers [8,9] under the assumption that energy transfers between the Chls occur by the Förster mechanism.

Such an identification can be provided by correlating the simulation results with the observations obtained in the recent sub-picosecond time resolved measurements. To meet our objective it is necessary to implement the theoretical tools on the computer. This implementation has been one of the major developments of this thesis.

This thesis is arranged as follows: Chapter 2 consisting of three sections offers some review to set up the background. The current structural knowledge of LHCII and a review of the current state of experimental information relevant to this thesis are summarized in sections 2.A and 2.B, respectively. The Pauli master equation formalism which is used to describe the time evolution of the excitations in the LHCII has been discussed in section 2.C. A brief description of the Förster mechanism has also been given in the same section. Chapter 3 describes the details of our implementation of the Pauli master equation formalism on the computer and also the development of the procedures to compare our simulation results with the current experimental results. Chapter 4 contains our simulation results, their subsequent analysis, and a discussion of the possible energy transfer pathways in LHCII.

CHAPTER 2

REVIEW

2.A The current structural model of the LHCII

A large part of the LHCII structure has recently been modeled by electron diffraction on two-dimensional crystals at atomic resolution by Kühlbrandt and co-workers [7].

The complex in the crystalline state forms trimers with three symmetrically (C_3) arranged monomers. The arrangement of the polypeptide (helices) and the pigments (chlorophylls and carotenoids) in one of the monomeric subunits are shown in Figure 2.1 and a view of the pigment arrangement in the trimer is given in Figure 2.2.

Biochemical studies reveal that each monomer contains a polypeptide consisting of 232 amino acids. In the current model, only 125 of the amino acids have been identified. The polypeptide consists of three transmembrane helices, A, B, and C, and another helix D that is roughly oriented parallel to the inner surface of the photosynthetic membrane. The helices A and B are related to each other by an approximate two-fold

symmetry axis that runs perpendicular to the plane of the membrane. The helices A and B form an X-like cross-bridge in the center of the complex. The helix C located at the side of this symmetrical core is believed to be an evolutionary addition.
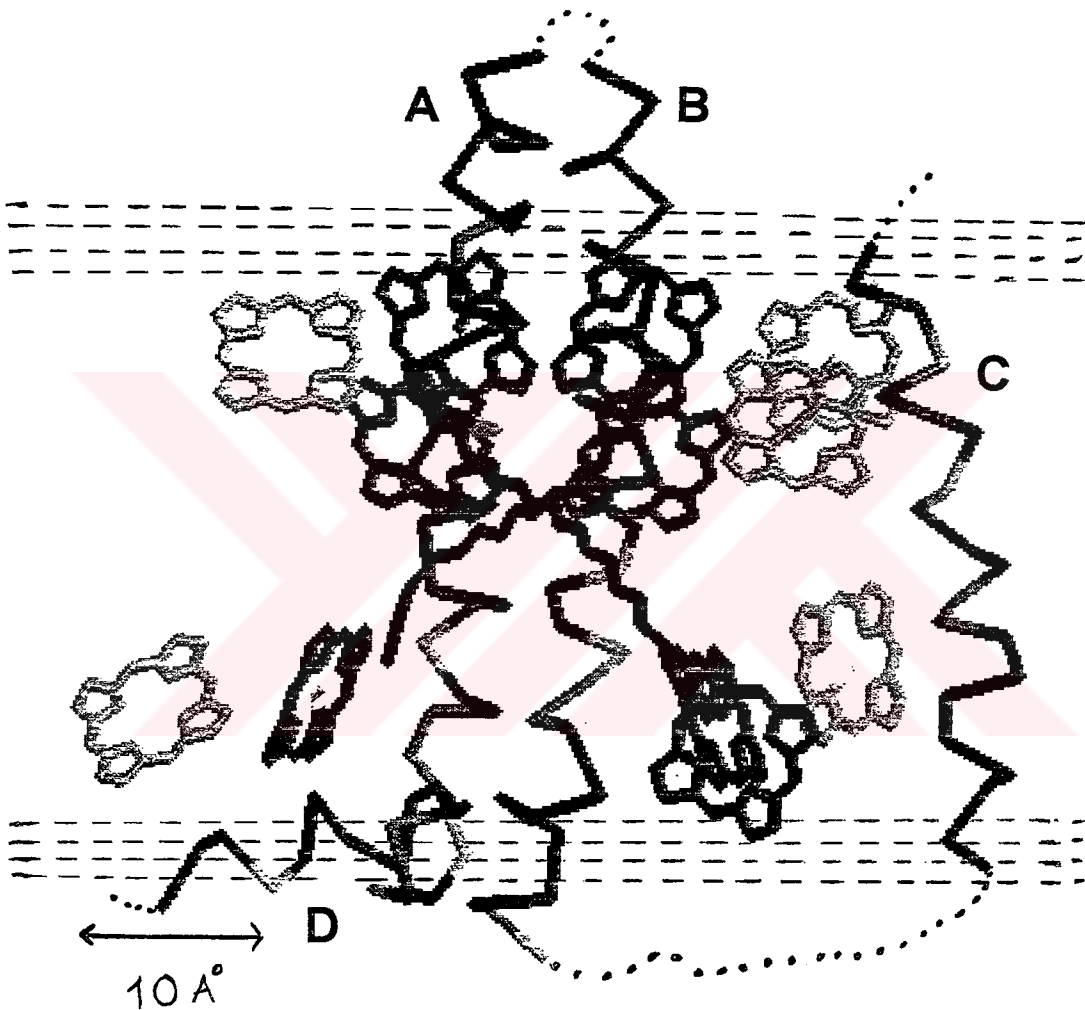
Figure 2.1.a: Side view of the arrangement of the pigments and helices in a monomer of LHCII.

Dashed lines indicate the approximate position of the photosynthetic membrane. Unresolved parts of the polypeptide chain connecting the helices A-D are drawn in dots. Two linear molecules in the center are Luteins. Chls *a* are black and Chls *b* are gray. A scale is provided to give an idea about the size of the complex. Created using the Molecular Graphics software RASMOL v.2.5.
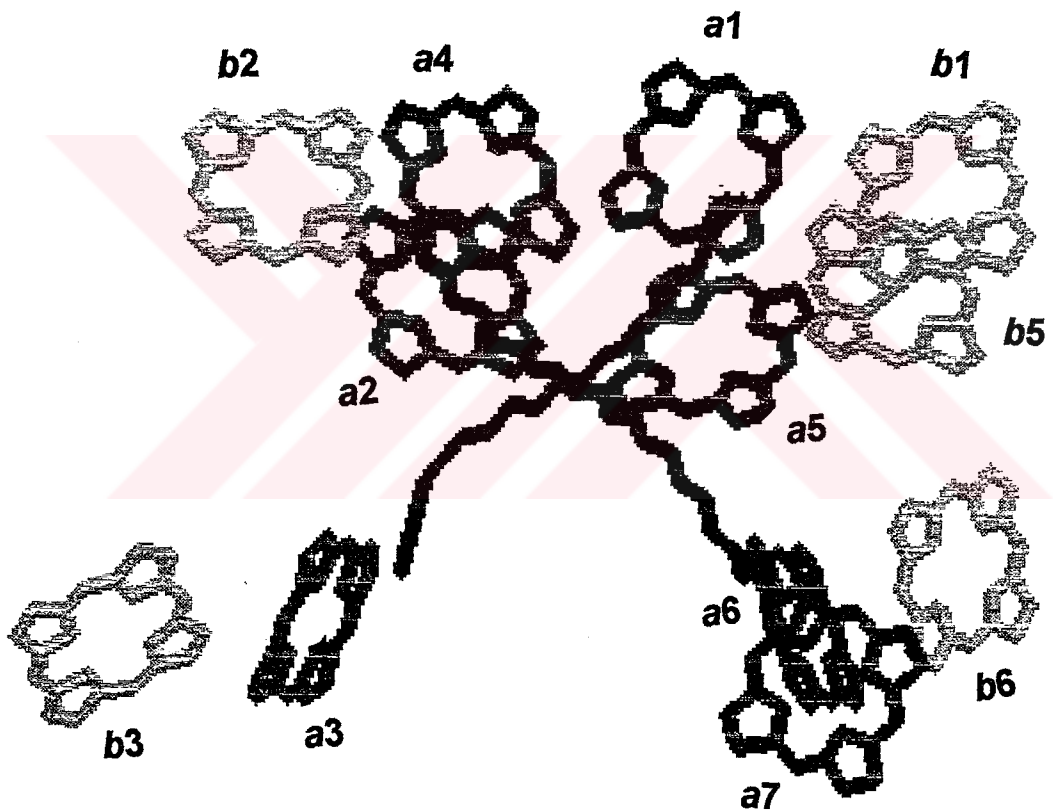
Figure 2.1.b: Side view of the arrangement of the pigments in a monomer of LHCII.

The helices of Figure 2.1.a are stripped off. The Chl molecules are assigned and labeled following Kühlbrandt *et. al.* [7].

Figure 2.2: Top view of the pigment arrangement in the trimeric LHCII.

C_3 symmetry axis is perpendicular to the plane. Color coding: Chl *a* and Lutein (black); Chl *b* (gray)

In each monomer, 2 carotenoids (Cars) and 12 Chls are bound to the helices. The Cars are identified as Luteins and they are located in the grooves created by the X-like crossing of the helices A and B. Having Cars, Chl *a*, and Chl *b* as its pigments, the complex absorbs the sun light over a wide range of the visible spectrum. The biochemical studies yield a Chl *a* to Chl *b* ratio of 1.3. At the current resolution (3.4 A°) Chls can only be modeled as naked tetrapyrrole rings. Therefore, definitive assignments of the identities of the Chls, as Chl *a* or Chl *b*, and the directions of the transition dipole moments associated with the electronic states responsible for energy transfer are not possible. The structure of a fully resolved Chl molecule is given in Figure 2.3. A tentative assignment of the pigment identities has been suggested by Kühlbrandt and co-workers [7] based on the stoichiometry and the functional aspects of the complex. Seven of the Chls which are in close contact with the Cars are assumed to be Chls *a*. The remaining five, each of which is in close proximity to a 'Chl *a*' molecule, are assumed to be Chls *b*. This assignment provides a molecular arrangement for rapid energy transfer from Chl *b* to Chl *a* and efficient quenching of Chl *a* triplets by Cars to reduce the yield of harmful singlet oxygen production.

The Chls are roughly arranged in two levels near the outer (upper) and the inner (lower) surfaces of the photosynthetic membrane. The upper level is a 'ring' of seven Chls and the lower one contains five Chl molecules. The center-to-center distances between the Chls in different levels are longer than 20 A°. The center-to-center distances between the closest Chl *b* and Chl *a* molecules range from 8.3 to 10.5 A°. The Chl porphyrin rings are

oriented roughly perpendicular to the membrane surface. The Chls of the three pairs in the upper level, *a1-a4, a2-a5, b2-b5,* and of the *a3-a6* pair in the lower level are related by an approximate two-fold symmetry.
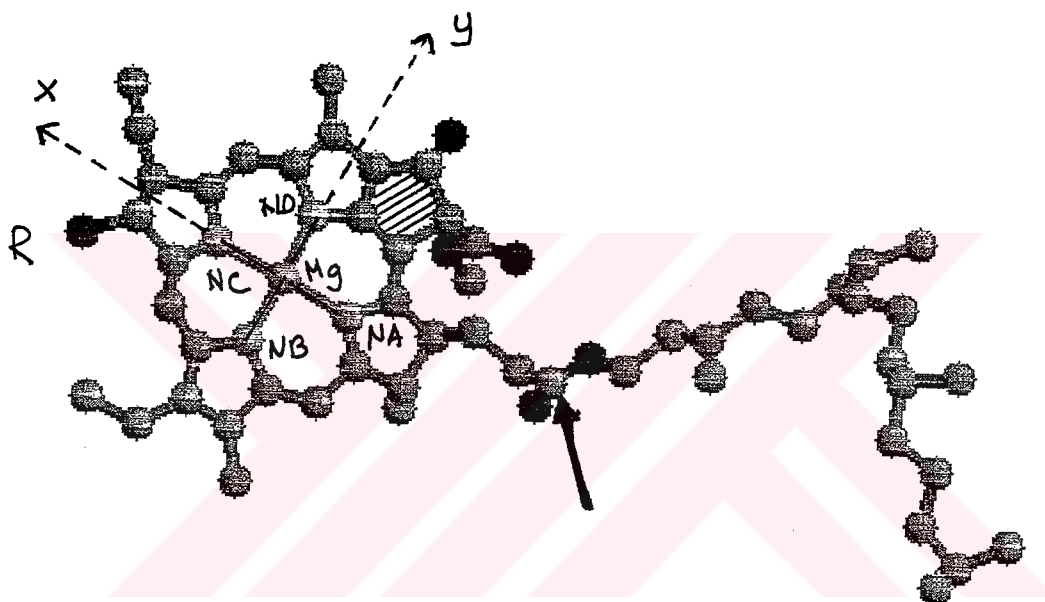
Figure 2.3: Structure of a Chl molecule.

There are two parts of a Chl molecule: the tail to the right of the arrow in the middle (phytyl chain) and the 'planar' head (porphyrin ring) in which the magnesium (Mg) atom at the center coordinates the four nitrogens, NA, NB, NC and ND. Nitrogens are labeled in the PDB (Brookhaven Protein Data Bank) format. Darker and lighter atoms are respectively Oxygen (O) and Carbon (C). Hydrogen (H) atoms are not tagged and the bond structure is not specified. The Vth ring is shaded. Chemical compositions of Chl *a* and Chl *b* molecules differ in the position indicated by R. The group R is CH_3 in Chl *a* and CHO in Chl *b*. The molecular axes x and y are defined along the diagonals connecting the nitrogens NA-NC and NB-ND. At the current resolution Chls of LHCII can only be modeled as naked tetrapyrrole rings (i.e., porphyrin without the Vth ring, the R group and the phytyl chain). Therefore neither their identity nor the molecular axes can be distinguished.

9

2.B Sub-picosecond time-resolved measurements of Chl *b* to Chl *a* energy transfer processes

The dynamics of energy transfer in LHCII have been studied extensively in the frequency domain [10-17] and in the time domain in sub-picosecond scale [18-23].

In this section, we will summarize the information provided by the recent sub-picosecond time-resolved experiments on the energy transfer processes from Chl *b* to Chl *a*.

The absorption spectrum of LHCII preparations at 77 K is shown in Figure 2.4 [10]. The absorption maxima of Chl *a* ($\approx$675 nm) and Chl *b* ($\approx$650 nm) are separated by 25 nm ($\approx$70 meV). LHCII is therefore an excellent system for the energy transfer studies. Chl *a* and Chl *b* can be selectively excited and the dynamics in either the Chl *a* spectral region or the transfers from Chl *b* to Chl *a* can be monitored.

Fluorescence up-conversion [18,19] and one- and two-color transient absorption [24] are the main techniques and the current time-resolution is around 150-250 fs. An experimental decay curve to illustrate the time scale of the decay of the Chl *b* excitation probability is given in Figure 2.5.

The results of the sub-picosecond experiments on the *b* to *a* transfer processes are collected in Table 2.1. The details on the experimental conditions are also given for each case in this table. In the pioneering study of Eads *et. al.* [18] the rise time of the Chl *a* fluorescence upon selective excitation of Chl *b* in the LHCII of *C. Reinhardtii* has been
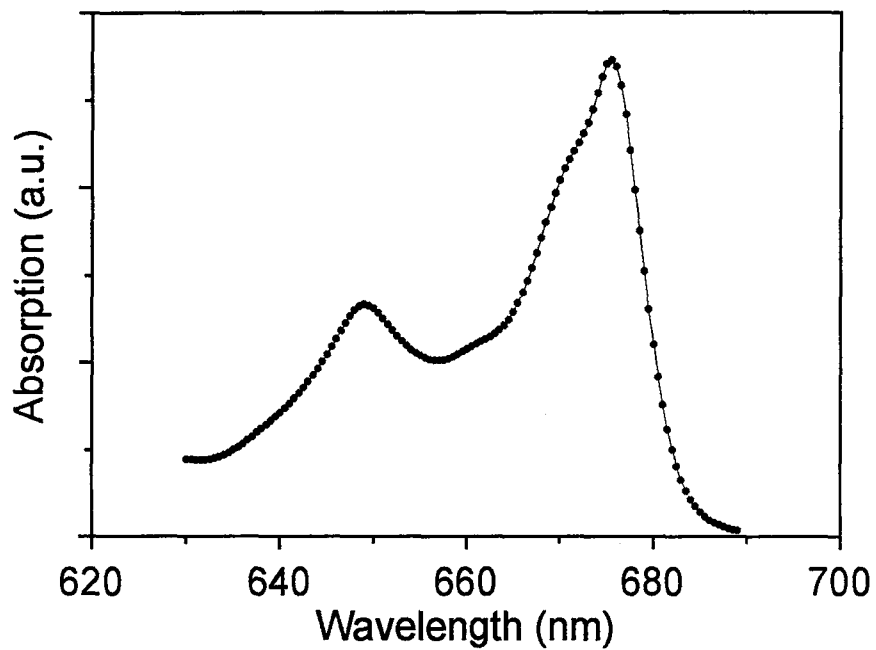
Figure 2.4: Absorption spectrum of LHCII at 77 K.

Chl *a* and Chl *b* absorption maxima are respectively around 675 nm and 650 nm. Data points are taken from ref. 10.
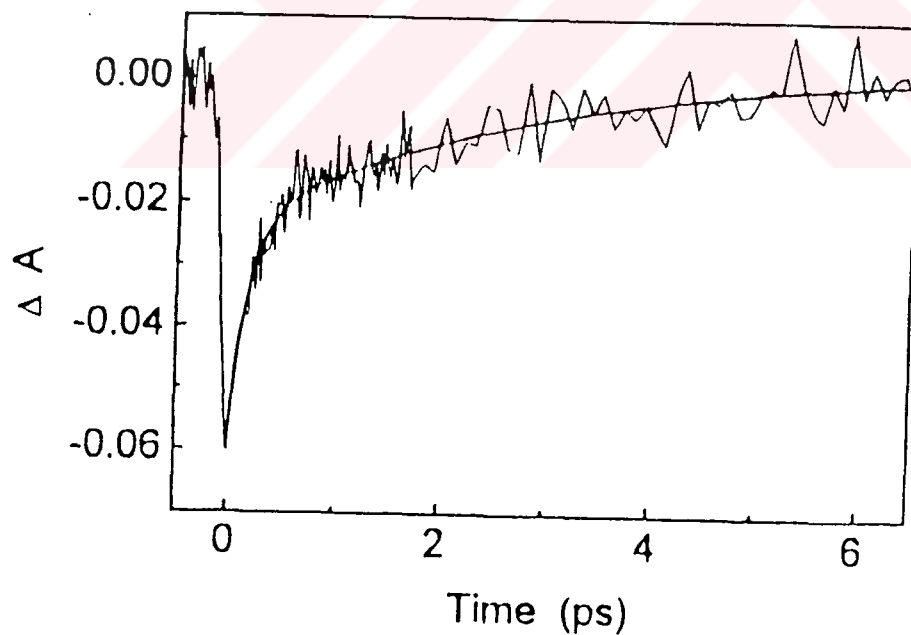
Figure 2.5: Transient absorption changes of LHCII in the Chl *b* spectral region.

Figure is taken from ref. 21.

measured. It has been established that *b* to *a* transfers occur in the subpicosecond scale (0.5 ± 0.2 ps). With improved resolution, Du *et. al.* [19] have detected two phases in the decay of fluorescence anisotropy: one of lifetime 0.25-0.30 ps and a slower decay around 5 ± 2 ps. The fast process has been interpreted to have some *b-b* contribution in addition to *b* to *a* transfers. The slow process has been attributed to the transfers among the Chl *b* molecules. One-color transient absorption study of Pallson *et. al* [20] has detected a 0.5 ps component (80%) by measuring the decay of Chl *b* absorption. This decay has also displayed a component of time constant around 2 ps (20%) which has been assigned to redistribution of excitation energy between different spectral forms of Chl *a*. A very fast (≈0.15 ps) *b* to *a* transfer time has been reported by Bittner *et. al.* [21] by measuring a very fast decay of Chl *b* absorption (0.16 ± 0.02 ps) and a similar rise time (0.145 ± 0.02 ps) of Chl *a* absorption in two-color transient absorption measurements. Chl *b* decay and Chl *a* rise data have also displayed a slower component (5 ± 2 ps). The relative contributions have been given as 65% (fast) and 35% (slow). Some part of the slow component has been attributed to transfers between Chls *a*. Chl *b* band was excited at 645 nm. In a more recent experiment by the same group, excitation of the Chl *b* band at 640 nm [22] (farther from the absorption maximum) have resulted in a fast (0.31 ps) and an intermediate (1 ps) component for transfers from Chl *b* to Chl *a*. Two-color transient absorption measurements by Visser *et. al.* [23] at 77 K have probed the Chl *b* decay/Chl *a* rise times in a broad range of wavelengths from 630 to 700 nm by exciting at the peak of Chl *b* absorption

Table 2.1: Ultrafast measurements of Chl *b* to Chl *a* transfers in LHCII.

Reference	System/ Temperature/ Pulse-spectral width/ Technique	Measurement	Lifetimes (ps)	Interpretation
Eads *et. al.* ref. 18 (1989)	*C.reinhardtii* / Room temp./ 500 fs –4 nm/ Fluorescence up-conversion	1. Rise of the Chl *a* fluorescence 2. Decay of the Chl *b* anisotropy (pump:650, probe:682-730 nm)	0.5± 0.2 < 1	*b-a* *b-a*
Du *et. al.* ref. 19 (1994)	*C.reinhardtii* / Room temp./ 100 fs–4 nm/ Fluorescence up-conversion	1.Rise of the Chl *a* fluorescence 2.Decay of the Chl *b* anisotropy (pump:650, probe:682-700 nm)	0.25-0.30 0.25-0.30 5-12	*b-a* & *b-b* *b-a* *a-a*
Pallson *et.al.* ref. 20 (1994)	Spinach LHCII/ Room temp./ 100 fs–4nm/ One-color transient absorption	1.Decay of the Chl *b* absorption at 650 nm 2.Decay of the 'Chl *a*' absorption at 665 nm	0.5 (80%) 2.0 (20%) 2.0 (25%) 15-20 (75%)	*b-a* *a-a* *a-a* *a-a*
Bittner *et.al.* ref. 21 (1994)	Spinach LHCII/ Room temp./ 130 fs -12 nm/ Two-color transient absorption	1.Decay of the Chl *b* absorption (pump:645 nm, probe:655 nm) 2.Rise of the Chl *a* absorption (pump:645 nm, probe:680 nm)	0.16±.02 (65%) 5±2 (35%) 0.145±.02 5±2	*b-a* *b-a* & *a-a* *b-a* *b-a* & *a-a*
Bittner *et. al.* ref. 22 (1995)	Spinach LHCII/ 12K and RT/ 130 fs-12 nm/ Two-color transient absorption	1.Rise of the Chl *a* absorption (pump:640, 665<probe<674 nm) 2.Rise of the Chl *a* absorption (pump:640, 675<probe<686 nm)	0.31 0.31 1.0 14.0	*b-a* *b-a* *b-a* & *a-a* *a-a*
Visser *et. al.* ref. 23 (1996)	Spinach LHCII/ 77 K/ 250 fs-3-4 nm/ Two-color transient absorption	Decay of the Chl *b* and rise of Chl *a* absorption (pump:649, 630<probe<700 nm)	<0.3 (42%) 0.6 (41%) 4-9 (17%)	*b-a* *b-a* *b-a*

*refers to the LHC of *C.reinhardtii* PSI and PSII double deficient-mutant

(649 nm). Three distinct Chl *b* to Chl *a* transfer times have been reported with lifetimes of <0.3 ps, ≈0.6 ps, and around 4-9 ps with respective amplitudes of around 40%, 40%, and 20%.

2.C Formalism

2.C.1 The Pauli master equation

The system under consideration is a network of N molecules arranged arbitrarily in space among which the electronic excitation energy flows due to the existence of the intermolecular interactions. In addition to the energy transfer among the molecules of the system, the radiative and the intermolecular non-radiative processes (other than energy transfer) are also possible. The objective is to describe the time evolution of the excitations created in such a system. The Pauli master equation (PME) formalism can be used to achieve this objective [25-27]. The occupation probabilities of the individual molecules obey the following PME

$$\frac{dP_i(t)}{dt} = -k_i P_i(t) - \sum_{\substack{j=1 \\ i \neq j}}^{N} F_{ji} P_i(t) + \sum_{\substack{j=1 \\ i \neq j}}^{N} F_{ij} P_j(t). \tag{2.1}$$

In Equation 2.1, $P_i(t)$ is the time dependent probability of finding the excitation on the ith molecule at time t, $k_i = k_{fi} + k_{ni}$ is the rate of decay due to

radiative (k_{fi}) and intramolecular nonradiative (k_{ni}) decays, F_{ji} is the rate of energy transfer from molecule i to molecule j. The first and second terms in Equation 2.1 represent the decay of the excitation probability on molecule i and the last term corresponds to excitation flow into molecule i from all the other molecules. The decay of excitation is accompanied by an equilibration of the excitation energy among the molecules of the system. No source term is included in Equation 2.1. Excitations are created by the initial conditions.

The set of N coupled linear differential equations for a network of N molecules can be put in a more convenient form by introducing the following energy transfer matrix, W, whose elements are

$$W_{ii} = k_i + \sum_{j=1}^{N} F_{ji} \qquad \text{(2.2.a)}$$

and

$$W_{ij} = -F_{ij} \qquad (i \neq j). \qquad \text{(2.2.b)}$$

Equation 2.1 then becomes

$$\frac{dP(t)}{dt} = -WP(t) \qquad \text{(2.3)}$$

where P(t) is an Nx1 matrix of site occupation probabilities and W is an NxN matrix of the kinetic processes. The formal solution to Equation 2.3 is

$$P(t) = G(t).P(0) \qquad (2.4)$$

where the matrix elements of P(0) are the initial distribution of excitations and G(t)=exp(-Wt). The matrix elements of G(t) give the conditional probability that the excitation occupies the ith site at time t given that it occupied the jth site at t=0. In other words, G(t) evolves the initial distribution of excitations created by optical absorption into the distribution at time t. The matrix elements of G(t) are:

$$G_{ij}(t) = S_{ik}e^{-\lambda_k t}S_{kj}^{-1} \qquad (2.5)$$

Here, λ_k are the elements of the diagonal matrix of the eigenvalues of W i.e., $\lambda = S^{-1}WS$ and S_{ik}'s are elements of the corresponding eigenvector matrix.

The matrix elements of Equation 2.3 or the solution to the PME (Equation 2.1) finally assumes the following form:

$$P_i(t) = \sum_{k=1}^{N}\sum_{j=1}^{N} S_{ik}e^{-\lambda_k t}S_{kj}^{-1}P_j(0) \qquad (2.6)$$

In summary, once the energy transfer matrix (W) is constructed, the objective of determining the time evolution of the site occupation (excitation) probabilities is reduced to solution of the eigenvalue problem represented by $WS = \lambda S$ and to the use of proper initial conditions.

2.C.2 Förster formula

The rate of energy transfer (F_{ji}) from the ith molecule to the jth molecule which interact through their transition dipole moments can be calculated using the Förster formula given below.

A quantum mechanical derivation for the energy transfer rate has been given by Förster in 1948 [28]. We suggest references [2,6,26,27] for more on the physics of the Förster transfer.

Förster rate from an initially excited molecule (donor, i) to an initially unexcited molecule (acceptor, j) which are separated by R_{ij} is given by

$$F_{ij} = C_{ij} \, \kappa_{ij}^2 \, R_{ij}^{-6} n^{-4} \tag{2.7}$$

κ_{ij}^2 depends on the orientations of the transition dipole moments and is given by $\kappa_{ij}^2 = [\, \hat{\mu}_i \cdot \hat{\mu}_j - 3(\hat{\mu}_i \cdot \hat{R}_{ij})(\hat{\mu}_j \cdot \hat{R}_{ij})\,]^2$. Here $\hat{\mu}_i$ and $\hat{\mu}_j$ are the unit vectors in the direction of the transition dipole moments. $\hat{R}_{ij}$ is the unit vector along the line connecting the 'centers' of the two molecules. n is the refractive index of the medium. C_{ij} is the overlap integral between the

donor's emission (J_i) and the acceptor's absorption (ε_j) spectra and is

proportional to $\int\limits_{0}^{\infty} J_i(v)\, \varepsilon_j(v)\, v^{-4}\, dv$ where v is the frequency.

CHAPTER 3

SCOPE, OUTLINE, AND PRELIMINARY RESULTS

3.A Scope

The main objective of this thesis has been the development of a set of tools that can be used to identify the energy transfer processes in a network of molecules (or states) such as in the LHCII. The tools developed are then used to address the following question: Can we identify the energy transfer pathways leading to the ultrafast processes in LHCII observed upon selective excitation of the Chls b of the complex [18-23] within the current conformational assignment of Kühlbrandt $et.$ $al.$ [7] and the most likely configurational assignments of Gülen $et.$ $al.$ [8,9] by assuming Förster mechanism [28] as the mechanism of energy transfer? A possible point of departure to answer this question is the simulation of the time evolution of the excitation probability on the Chls b of the system and a subsequent multi-exponential analysis of this evolution.

The assumptions already built in the question we have asked are:

• Energy transfer between all Chl a- Chl a, Chl b- Chl b, and Chl b- Chl a

pairs of the LHCII are of Förster type.

- Assignment of Kühlbrandt and co-workers on the Chl identities (the Kühlbrandt conformation) is accepted.

- Assignment of the dipole moment directions of Gülen and co-workers (the most likely configurations) is used.

We further impose the following assumptions:

- All Chl *b (a)* molecules of the system are spectrally equivalent.

- Upon selective excitation of the Chl *b* region (640-650 nm), all Chls *b* are uniformly excited whereas none of the Chl *a* molecules (or Chl *a* states) absorbing maximally around 670-675 nm are excited.

We refer to a recent study by Visser *et. al.* [23] for a nice discussion on the justification of the assumptions given above.

Under these assumptions, the quantity we want to study can be written as:

$$P_b(t) = \sum_{bi} P_{bi}(t) \tag{3.1}$$

where the summation is over all Chl *b* molecules. Each term in the summation represents the evolution of the site occupation probability on an individual Chl *b* molecule in the system as defined by Equation 2.1 (5 Chls/monomer and 15 Chls/trimer).

The system will evolve with a number of rates equal to the number of distinct eigenvalues of the energy transfer matrix W (Equation 2.2). In principle all the eigenvalues of W will contribute to the decay of each site

occupation probability. Time evolution of each of the site occupation probabilities is a linear combination of the exponential decay terms with the rates (time constants) given by the eigenvalues of the energy transfer matrix W. The contribution of each distinct decay component to the evolution (its amplitude) will however be decided by the pump and probe conditions. In other words, time evolution is always governed by the same eigenvalue problem, but the amplitude contribution of each decay component to a specific observable depends on the pump and probe conditions (Equation 2.6)

$$P_b(t) = \sum_n B_n \exp(-t/\Gamma_n) \quad n=1,2,3. \tag{3.2}$$

where $\Gamma_n = 1/\lambda_n$.

In principle it is possible to discuss the contribution of each eigenvalue to the decay characteristics observed in a specific experiment. However as we have already mentioned in section 2.B, upon selective excitation of Chls b, at most three components could be resolved by the experimental studies. We therefore have decided to analyse the decay of the Chl b excitation in terms of a limited number of exponentials to extract information at the same level with the experimental predictions and use this information for a more detailed understanding of the energy transfer pathways in the LHCII.

3.B Outline of the calculations

To meet the objectives described above, the formalism reviewed in section 2.C needs to be implemented on the computer. We have carried out a three-step task for this implementation.

Step 1: Estimates for the Förster rates between all the Chl pairs in LHCII (Equation 2.7), setting up the energy transfer matrix (W) (Equation 2.2), and formation of the PME (Equation 2.3) describing the time evolution of the site occupation probabilities.

Step 2: Solution of the PME for the site occupation probabilities and simulation of the time dependence of the observables (Equation 3.1).

Step 3: Multi-exponential analysis of the simulated time evolution of the observables.

The numerical procedures for step 1 are developed in the FORTRAN language (Fortran77 v3.20, Copyright Microsoft Corp.). For steps 2 and 3, MATLAB v.4.0 environment is preferred for its ease, efficiency, and speed in matrix calculations (MATLAB is a registered trademark of the Math Works Inc.). The eigenvalue problem of step 2 is solved by using the MATLAB procedure EXPM and the solutions for the site occupation probabilities are used in coding the experimentally observed quantities again in the MATLAB environment. The MATLAB procedure FUNFIT is utilized for the multi exponential analysis of step 3. All the codes are original to this thesis and all the simulations are carried out on an IBM compatible PC486. A flowchart of the calculations is given in Appendix.

3.B.1 Estimate of the Förster rates

The crucial input parameters for our calculations are the Förster rates. The rate of energy transfer from a donor (D) to an acceptor (A) molecule in the Förster formalism is given by Equation 2.7: $F_{AD} = C'_{AD} \kappa^2_{AD} R^{-6}_{AD}$ where we denote $C'_{AD} = C_{AD} / n^4$

a R and κ^2 calculations

Atomic coordinates which are kindly provided by Dr. Werner Kühlbrandt allows the calculation of the geometrical factors κ^2 and R. The Chl molecular structure shown in Figure 2.3 is referred for the nomenclature used below.

It is straightforward to calculate the center-to-center (Mg-to-Mg) distances between a pair of Chls.

To calculate κ^2, it is necessary to define the directions of the transition dipole moments that resonate the energy transfer in the spectral region of interest. The spectral region between 640-680 nm is termed as the Q_y band and in this band Chl b (a) absorbs maximally around 650 (675) nm (see Figure 2.4). The dipole moment direction associated with the Q_y transition of each Chl (a or b) molecule is suggested to be approximately along the molecular y-axis connecting the nitrogens NB and ND [30]. In the current atomic model, the resolution is not sufficient to identify the positions

of the phytyl chain and/or the positions of the Vth ring and the chemical group i.e., the Chls are modelled as naked tetrapyrrole rings. Consequently, the molecular x- (NA-NC) and y- (NB-ND) axes cannot be distinguished. There is therefore a binary ambiguity for the Q_y transition dipole moment direction of each of the 12 Chls in LHCII. In the rest of this thesis, we shall denote these two possible directions as states 1 and 0. State 1 is defined along NB-ND and state 0 is defined along NA-NC in the convention of the file containing the atomic coordinates provided by Dr. Werner Kühlbrandt. This binary directional assignment leads to four orientational combinations for calculating the κ^2 factor for any D-A pair: 1-1; 1-0; 0-1; 0-0.

b Estimate of the C coefficients

The C_{AD} coefficients for the Chl a-Chl a (C_{aa}), Chl b-Chl b (C_{bb}), Chl b-Chl a (C_{ab}) and Chl a-Chl b (C_{ba}) pairwise transfers are estimated by using the method suggested originally by Shipman and Hausman [31] and later modified by Jean et. al. [32].

We have prefered this method since it provides an analytical form in which the effects of several parameters involved in determination of C_{AD} can be easily followed. The analyticity is brought in by approximating the absorption and emission spectra as symmetric Gaussians.

Each symmetric Gaussian spectrum is defined by a width (σ), a peak wavelength (λ), and a transition dipole strength (μ). If the spectra are

assumed identical in shape it has been shown [18] that for a Chl pair whose emission and absorption maxima are separated by Δ;

$$C_{AD} = \mu_A^2 \cdot \mu_D^2 \cdot I_{AD} \tag{3.5}$$

where $I_{AD} = \text{constant} \cdot \dfrac{1}{\sqrt{2\pi(\sigma_A^2 + \sigma_D^2)}} \cdot \exp[-\Delta_{AD}^2 / 2(\sigma_A^2 + \sigma_D^2)]$

in which the constant in front is 29.99 Debye^{-4}.ps^{-1}.nm^6.cm^{-1}.

No reliable *in vivo* values for most of the parameters are available, we therefore give an estimate using the parameters based on the absorption/emission data of Chls in solution at room temperature [18,31]. The spectral widths (σ) are taken as 135 and 145 cm^{-1} respectively for Chl *a* and Chl *b* and we take $\Delta_{aa}=\Delta_{bb}=110$ cm^{-1}, $\Delta_{ab}=275$ cm^{-1} and $\Delta_{ba}=495$ cm^{-1}. We then find $I_{aa}=0.05310$, $I_{bb}=0.05054$, $I_{ba}=0.02305$ and $I_{ab}=0.0026$. Note that bigger the delta less the overlap. We have also tried several other delta sets and found that I_{DA} is not too sensitive to the choice of the Δ's: ± 10 cm^{-1} changes in Δ's change I_{DA}'s by less than 5%.

If we take the μ^2 values in CCl$_4$ $\mu_a^2=24.65$ Debye^2 $\mu_b^2=16.91$ Debye^2 [33], we find that $C_{aa}=32.26$, $C_{bb}=14.45$, $C_{ba}=9.61$ and $C_{ab}=1.11$ nm^6/ps. Notice that all factors being equal *a-a* provides the fastest transfer.

We have first checked whether the C values given above have the correct order of magnitudes. For this purpose we have estimated the

transfer rates by using average distances that we have calculated for the closest *a-a*, *b-b*, and *b-a* pairs: R_{ba}=0.85-1 nm, R_{aa}=R_{bb}=1.2-1.5 nm. By taking κ^2=1 and n=1.5, we find 1/F_{ab}= 200-500 fs, 1/F_{aa}= 500 fs-2 ps, and 1/F_{bb}=1-4 ps. These time constants have the same order of magnitudes with those observed experimentally. Notice that short distances beat poor overlaps.

Some earliear calculations when translated into C_{AD} coefficients give (in nm^6/ps): C_{aa}=15.05, C_{bb}=6.76 [18], C_{aa}=14.94, C_{bb}=6.70, C_{ab}=4.32 [34]; C_{aa}=21.38 [30]; C_{aa}=162.3, C_{bb}=79.4 and C_{ab}=54.3 [23,29]. Some part of the spread could be attributed to the use of different methods, but most of it is due to the use of different dipole strengths by different groups.

Another uncertainty in estimating the *in vivo* rates is the value of refractive index. The refractive indices used in calculating the Förster rates range from 1.33-1.36 [18,30,34] to 2.4 [23].

More relevant to our calculations are the ratios C'_{aa}/C'_{ab} and C'_{bb}/C'_{ab}. These ratios are independent of the refractive index. They depend on (μ_b^2/μ_a^2) for which a ratio of 0.7 is well-accepted [33]. Furthermore, as we have discussed above the only other parameter that is involved in the ratios, I_{AD}, is not particularly sensitive to the changes on the spectral parameters (σ and Δ). We have limited our calculations to a range of these ratios obtained using several data on C's given above. These ranges are: C'_{aa}/C'_{ab}=2.95-3.50 and C'_{bb}/C'_{ab}=1.45-1.55.

c Selection of the configurations

Since each Chl can either be in state 1 or in state 0 for a given molecular conformation (a particular assignment of the Chl identities) there are $2^{12}=4096$ possible configurations for the orientational arrangement of the transition dipole moments. Throughout the calculations the tentative molecular conformation of Kühlbrandt *et. al.* [7] shown in Figure 2.1.b and reviewed in section 2.A is used.

A method is recently developed by Gülen *et. al.* [8,9] to resolve the ambiguities in the Chl (dipole moment) orientations given a particular molecular conformation. This method explores the sensitivity of polarized absorption spectroscopy such as linear- and circular- dichroism on the molecular configurations. Upon application of this method to the Kühlbrandt conformation, it has been found that only a limited number of configurations can explain the key features of the polarized absorption spectra of LHCII [10].

The most likely orientations (1 or 0) for each of the twelve Chls are searched and a prediction has been made for the states of 8 out of 12 Chl molecules [8, 9]. The most likely state for five of the Chls *a* namely, *a1, a2, a4, a5* and *a7* is suggested to be 0. The state of the two remaining Chl *a* molecules (*a3* and *a6*) could not be determined. Following this suggestion the Chl *a* conformations (*a1 a2 a3 a4 a5 a6 a7*) are selected as: 0010010; 0010000; 0000010; 0000000. Of the five Chl *b* molecules in the system only *b3* is strongly biased to be in state 1. Although the bias was not as strong,

Chl *b*2 and *b*5 are also suggested to be in state 1. Then, the most likely Chl *b* conformations (*b*1 *b*2 *b*3 *b*5 *b*6) are: 01110; 01111; 11110; 11111.

The configurations we have studied below are those that are found to yield the best agreement with all the key features of the linear and circular dichroism spectra in which the 8 Chls discussed above are assumed to be in the most likely states predicted by Gülen *et. al.* [8,9]. These are: 3490 (0010010 11110); 3505 (0010010 01111); 3506 (0010010 01110); 3553 (0010000 11111); 3554 (0010000 11110); 3569 (0010000 01111); 3570 (0010000 01110); 4001 (0000010 11111); 4002 (0000010 11110); 4066 (0000000 11110); 4081 (0000000 01111); and 4082 (0000000 01110). We have also studied the configuration 3489 (0010010 11111) to compare with the results of Visser *et. al.* [23,29].

3.C Preliminary results

3.C.1 Förster rates in LHCII

The transfer rates (F_{AD}) between all Chl pairs in one of the monomers and in the LHCII trimer are calculated using the Förster formula. In Table 3.1, we have listed the transfer times ($1/F_{AD}$) between the important D-A pairs and the distances between the Mg atoms of these pairs in one of the monomeric units. The calculations are carried out for all four possible pairwise dipole moment orientations. The Förster parameters are: C'_{aa}=5, C'_{bb}=2.5, and C'_{ab}=1.67 nm^6/ps.

The information on the fastest intermonomer energy transfer processes are given in Table 3.2 (in the same convention as Table 3.1).

The major relations among the Chls of LHCII can be followed using Tables 3.1 and 3.2 (We shall comment on these relations later).

Table 3.1: Distances and transfer times between the important Chl pairs in the monomeric LHCII.

D	A	R (nm)	0-0	0-1	1/F (ps) 1-0	1-1
b1	a1	1. 052	0.65	3.52	18.45	0.52
b2	a1	1.724	8.56	168.79	10.86	13.97
b2	a2	0.830	0.23	0.27	0.22	0.57
b3	a3	0.916	1.13	0.81	0.27	0.71
b5	a4	1.751	8.06	27.06	15.32	38.77
b5	a5	0.891	0.32	7.45	5.46	0.29
b5	a6	1.968	71.69	43.54	inf.	11.14
b6	a6	0.876	4.45	0.48	0.19	1.40
b6	a7	1.001	0.74	0.61	0.29	18.56
a1	a2	1.232	0.98	0.54	1.14	1.87
a1	a5	1.940	10.67	inf.	inf.	9.04
a1	a6	1.948	13.97	inf.	9.81	5.12
a2	a4	1.737	5.39	inf.	inf.	4.66
a2	a6	2.028	4.15	51.73	inf.	inf.
a3	a5	2.132	5.22	inf.	inf.	inf.
a3	a6	2.173	inf.	18.83	18.86	inf.
a4	a5	1.269	1.16	1.07	1.41	2.04
a5	a7	1.578	3.49	16.13	105.35	0.88
a6	a7	1.158	1.16	2.59	1.68	0.60
b1	b5	1.057	0.85	19.74	6.79	0.55
b1	b6	1.521	84.91	2.81	5.05	5.12
b5	b6	1.461	2.43	5.52	2.20	352.73

The transfer times longer than 500 ps are indicated as 'inf.'. Only the shaded regions are acceptable within the dipole moment assignments of Gülen *et. al.* [8,9].

Table 3.2: Distances and transfer times of the fastest intermonomeric Chl pairs in the LHCII trimer.

D	A	R (nm)	0-0	1/F (ps) 0-1	1-0	1-1
a4	a5	2.595	50.76	55.16	inf.	68.06
a5	a3	2.077	50.74	32.46	131.42	34.70
a5	a4	1.644	16.23	74.42	19.05	7.36
a5	a5	1.833	93.50	128.36	172.12	4.09
a7	a3	1.694	71.61	127.73	6.48	16.19
b6	b3	1.994	61.67	68.40	301.64	inf.
b5	a4	1.716	inf.	26.30	10.56	425.15

3.C.2 Development of the simulation procedure

We have selected one of the configurations (3505) to discuss the development of our simulation procedure. The time evolution of the total probability on the Chl b molecules versus that on the Chl a molecules and the time evolution of the probability on the individual Chl b molecules in the monomeric LHCII are given in Figures 3.1 and 3.2, respectively. The Chls b are selectively excited with equal probability. The decay of the total probability on the Chls b is complemented by the rise of the total probability on the Chls a. The Förster parameters are selected such that the transfer from b's to a's is mainly complete in about 5 picoseconds as observed in the experiments (see Figure 2.5). The back transfers from Chl a to Chl b are neglected. We have estimated that at room temperature the a to b transfer rates are about an order of magnitude slower than the b to a

transfer rates (Chls b absorb about an energy $3k_BT$ higher than the Chls a).
At 77 K the energy separation is more than 10 k_BT.

We have also simulated the decay profiles for the trimeric LHCII. The monomeric and trimeric simulations are almost identical independent of the temperature (results are not shown). Therefore in the rest of the calculations we will use the results obtained with the monomers.

The characteristics of the two- and three- component exponential fits to the simulated decay of the total probability on the Chl b molecules are given in Figure 3.3. For this specific configuration a two-component fit is also satisfactory. However at least three components are needed for a satisfactory fit to the decay profiles of some of the other configurations we have studied. Apart from the considerations on the fit quality, the main reason for choosing a three-component exponential fit to the time evolution of the probabilities is to provide information at the same level with the current experimental results.

We shall denote the lifetimes of the three components as τ_1, τ_2, and τ_3 and their respective amplitudes as A_1, A_2, and A_3, and we refer to them as the fast, intermediate and slow components.

Table 3.3 shows the fit results for several different ratios of C'_{aa}/C'_{ab} and C'_{bb}/C'_{ab} while C'_{ab} is kept fixed. The ratios are picked within the range of values reported in the literature as discussed in section 3.B.1.b, i.e, C'_{aa}/C'_{ab}=2.95-3.50 and C'_{bb}/C'_{ab} =1.45-1.55. This table is provided in order to verify that the amplitude information part of the fit results remains

31

essentially unaltered if the ratios of the Förster parameters are limited to the ranges reported in the literature.
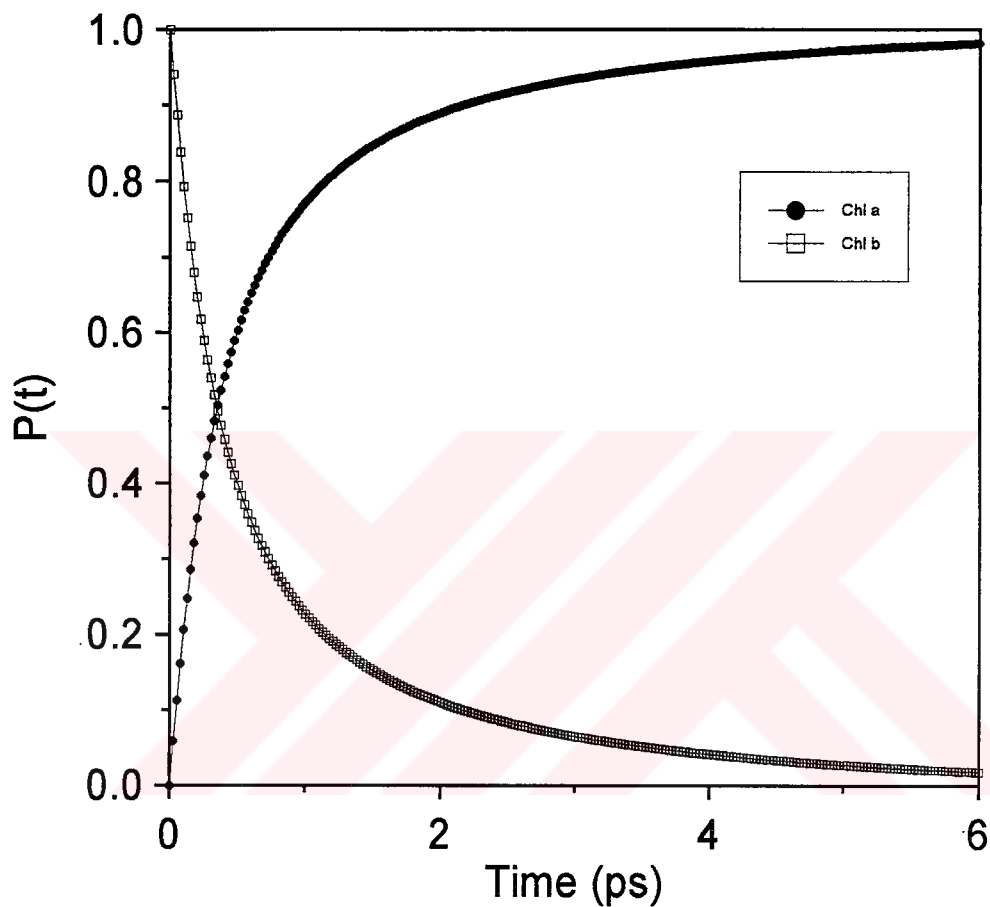

Figure 3.1: Time evolution of the total probability on the Chl *b* molecules versus Chl *a* molecules upon selective excitation of Chls *b*.

Decay of the total probability on the Chl *b* molecules, $P_b(t)$. Rise of the total probability on the Chl *a* molecules, $P_a(t)$. In the absence of processes other than energy transfer, $P_b(t)+P_a(t)=1$.
The configuration is 3505 ($a1=0$, $a2=0$, $a3=1$, $a4=0$, $a5=0$, $a6=1$, $a7=0$ and $b1=0$, $b2=1$, $b3=1$, $b5=1$, $b6=1$). The Förster parameters are: $C'_{aa}=5$, $C'_{bb}=2.5$ and $C'_{ab}=1.67$ nm^6/ps. The transfers from Chl *a* to Chl *b* and the processes other than energy transfer are ignored.
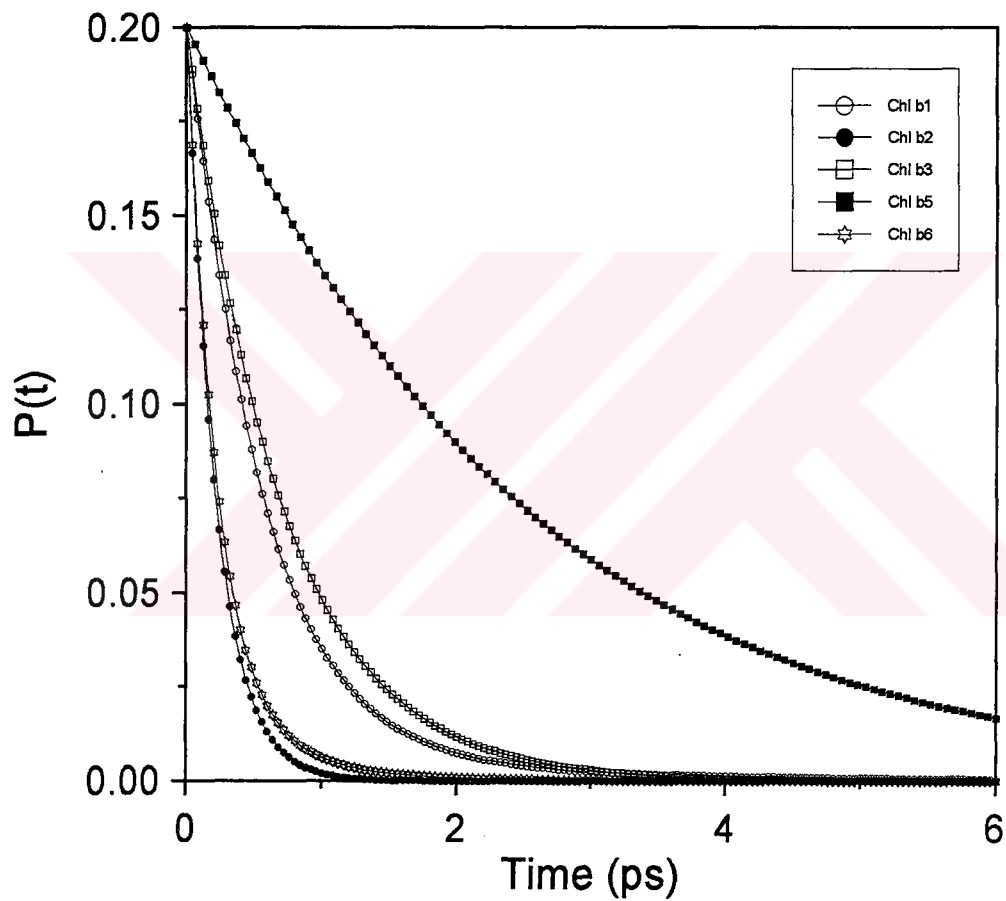
Figure 3.2: Time evolution of the probability on the individual Chl b molecules.

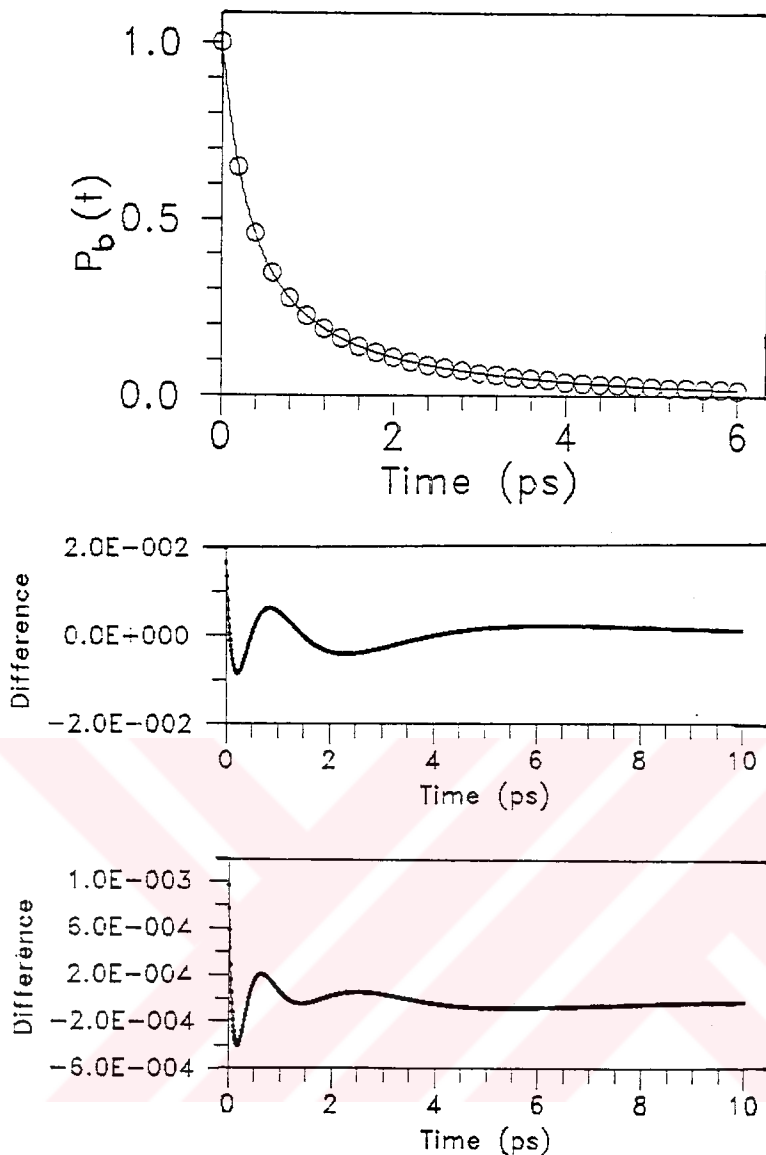The configuration and Förster parameters are the same as in Figure 3.1.

Figure 3.3: Comparison of the two- and three- component exponential fits to the time evolution of the total probability on the Chl *b* molecules.

The configuration and Förster parameters are the same as in Figure 3.1.
The top panel shows the simulation results obtained using Equation 3.1 (open circles) vs. the fit obtained using two or three exponentials (solid line). The simulation is carried out with 0.01 ps intervals and up to 10 ps. For clarity one out of every 20 simulation points is shown. The differences between the two exponential fits are not discernible on the scale of this panel. The data can be fit to a sum of two exponential terms with the transfer times of 0.350 and 2.014 ps with the respective amplitudes of 69% and 31%. Using three exponentials, one obtains the transfer times of 0.226, 0.620 and 2.387 ps with the respective amplitudes of 38%, 40% and 22%.
The middle panel shows the difference between the dots and the solids line of the top panel for the two-component fit. the average error is 0.0912.
The bottom panel shows the difference between the dots and the solid line of the top panel for the three-component fit. The average error is 0.0011.

Table 3.3: Fit results for several sets of Förster parameters with different C'_{aa}/C'_{ab} and C'_{bb}/C'_{ab} ratios.

C'_{aa}/C'_{bb}	C'_{bb}/C'_{ab}	τ_1 (ps)	τ_2 (ps)	τ_3 (ps)	A_1 (%)	A_2 (%)	A_3 (%)
3.50	1.55	0.221	0.604	2.356	37	41	22
2.95	1.45	0.221	0.606	2.373	37	41	22
3.50	1.45	0.222	0.626	2.502	38	41	21
2.95	1.55	0.222	0.625	2.491	38	41	21
3.00	1.50	0.221	0.605	2.364	37	41	22

The values of C'_{aa}, C'_{bb} and C'_{ab} are (nm^6/ps): 5.85, 2.59, 1.67 (1st set); 4.93, 2.42, 1.67 (2nd set); 5.85, 2.42, 1.67 (3rd set); 4.93, 2.59, 1.67 (4th set) and 5.00, 2.50, 1.67 (5th set).

We have also checked that the time scales of each of the decay components are mainly governed by b to a transfers. Then the decay can be safely scaled with the b to a transfer transfer time ($1/C'_{ab}$). The scaling can be easily observed by examining the fit results given in Table 3.4. Three different C'_{ab} values (1, 1.67, and 2 nm^6/ps) are considered while keeping $C'_{aa}/C'_{ab}=3$ and $C'_{bb}/C'_{ab}=1.5$. Fast, intermediate, and slow lifetime components scale (get shorter) by the amount of increase in the C'_{ab} parameters. Among these Förster parameter sets, the second one with $C'_{aa}=5$, $C'_{bb}=2.5$, and $C'_{ab}=1.67$ nm^6/ps compares best with the

experimentally observed lifetimes of the fast, intermediate and slow components.

Table 3.4: Scaling of the fast, intermediate and slow components with C'_{ab}.

C'_{aa}	C'_{bb}	C'_{ab}	τ_1 (ps)	τ_2 (ps)	τ_3 (ps)
	(nm^6/ps)				
3.00	1.50	1.00	0.369	1.009	3.937
5.00	2.50	1.67	0.221	0.605	2.364
6.00	3.00	2.00	0.185	0.509	1.976

CHAPTER 4

RESULTS, DISCUSSION, AND CONCLUSIONS

The characteristics of the three-component fits to the simulated decay of the total probability on the Chl b molecules for the selected configurations are shown in Table 4.1. Also shown in Table 4.1 are the lifetimes which dominate the decay of each Chl b molecule in the system. The dominant lifetime of each Chl b molecule is obtained by fitting each Chl b_i decay curve to a sum of two exponentials.

4.A Interpretation of the results

We would like to discuss the results presented in Table 4.1 and the possible roles of the Chls *in vivo* energy transfer in terms of the energy transfer pathways available to the Chls in each configuration. It is most appropriate to base this discussion on the compartmental nature of our configurations as opposed to the more interconnected nature of the configurations selected under the assumption that the nature takes the most

Table 4.1: Decay characteristics of the selected configurations.

codes*	τ_1 (ps) (A$_1$)	τ_2 (ps) (A$_2$)	τ_3 (ps) (A$_3$)	b1	lifetime (ps) b2	b3	b5	b6
3489 1111	0.221 (38%)	0.700 (20%)	2.645 (42%)	2.615	0.219	0.702	2.546	0.224
3490 1110	0.227 (33%)	0.696 (20%)	1.849 (47%)	2.615	0.219	0.702	2.546	0.224
3505 1101	0.221 (37%)	0.605 (41%)	2.364 (22%)	0.563	0.219	0.701	2.162	0.246
3506 1100	0.237 (36%)	0.724 (42%)	1.314 (22%)	0.608	0.219	0.702	1.700	0.249
3553 1011	0.142 (34%)	0.619 (24%)	3.314 (41%)	3.342	0.218	0.701	3.208	0.111
3554 1010	0.228 (23%)	0.639 (25%)	2.442 (52%)	2.449	0.218	0.702	2.250	0.426
3569 1001	0.142 (34%)	0.561 (44%)	2.969 (22%)	0.525	0.218	0.700	2.938	0.109
3570 1000	0.223 (22%)	0.615 (43%)	1.557 (35%)	0.606	0.218	0.701	2.324	0.448
4001 0111	0.237 (58%)	0.910 (0%)	2.627 (42%)	2.580	0.220	0.269	2.481	0.241
4002 0110	0.242 (53%)	1.807 (41%)	2.055 (6%)	2.094	0.220	0.269	1.843	0.241
4066 0010	0.259 (46%)	1.245 (4%)	2.468 (50%)	2.436	0.220	0.269	2.252	0.425
4081 0001	0.143 (37%)	0.399 (41%)	2.941 (22%)	0.531	0.220	0.269	2.896	0.109
4082 0000	0.243 (40%)	0.559 (25%)	1.555 (35%)	0.609	0.220	0.269	1.768	0.447

* In all configurations a1, a2, a4, a5, and a7 are in the state 0 and b2, b3, and b5 are in the state 1. The states of a3, a6, b1 and b6 are indicated below the codes of the selected configurations.

38

efficient pathways [34]. The compartmental nature of our configurations is first noted by Kiraly [34] and we are inspired by his discussion.

Compartment refers to a group of molecules that transfer to each other very fast (in the subpico-picosecond scale), but have slower transfers with the rest of the molecules in the system.

Based on this definition, we have identified the compartmental structure for each of the 13 configurations studied in this thesis using the pairwise Chl transfer times within a monomer listed in Table 3.1. A block diagram of the compartmental structure for each configuration is provided in Figure 4.1.

In terms of their compartmental compositons we can divide our configurations into two main classes. In both categories, there are five compartments within a monomer. Three of the compartments are common to both. These are:

Compartment 1: Chl *b*3 and Chl *a*3

Compartment 2: Chl *a*4 and Chl *a*5

Compartment 3: Chl *b*6, Chl *a*6, and Chl *a*7.

The other two compartments of the first class are;

Compartment 4a: Chl *a*1, Chl *b*2, and Chl *a*2

Compartment 5a: Chl *b*1 and Chl *b*5,

and those of the second class are;

Compartment 4b: Chl *b*1, Chl *b*2, Chl *a*2, and Chl *a*1
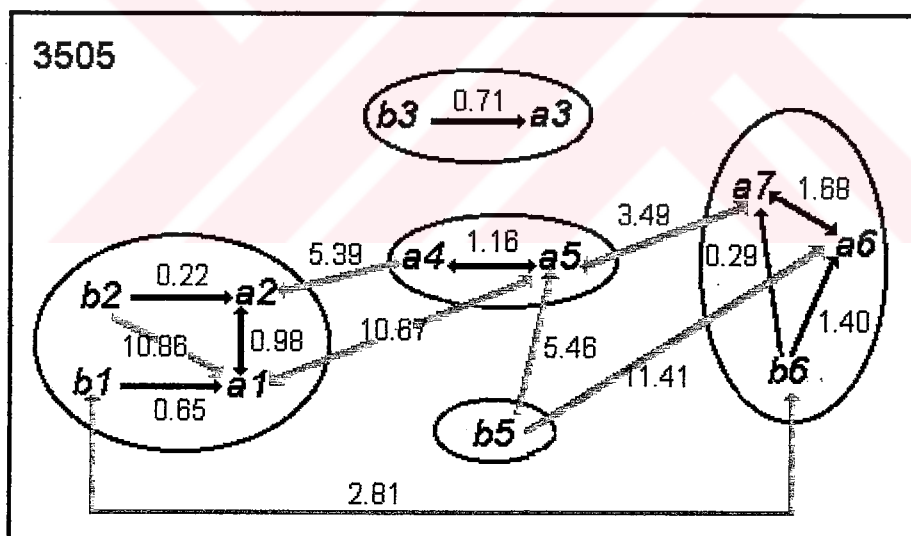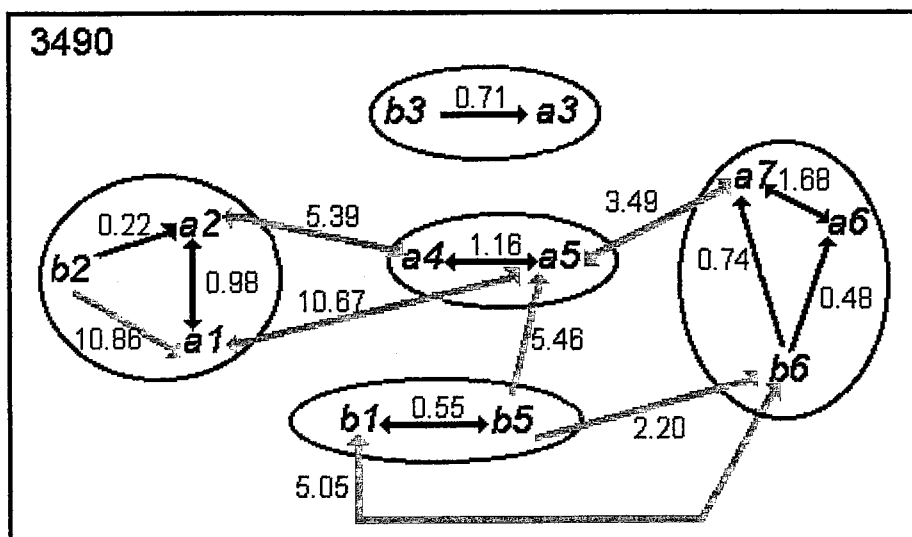
Compartment 5b: Chl *b*5.

Figure 4.1: Compartmental structures and energy transfer pathways of the selected configurations.

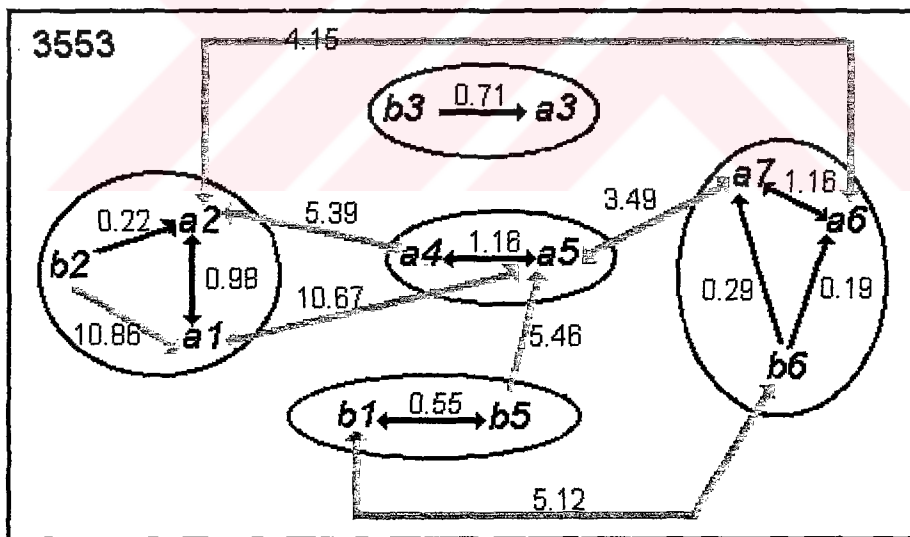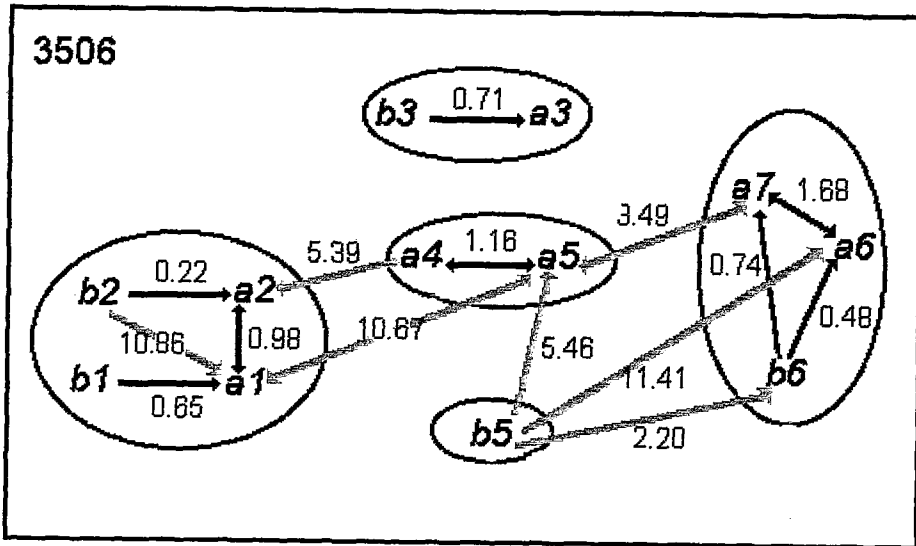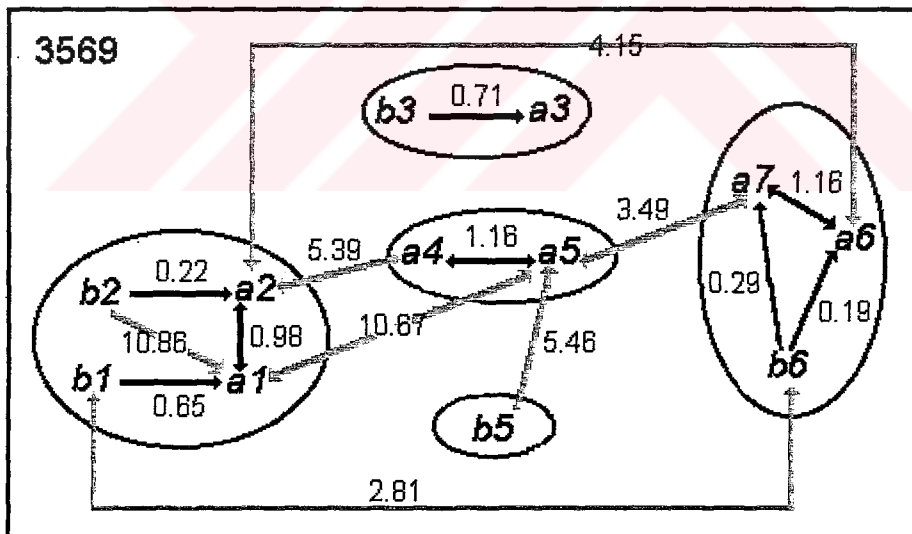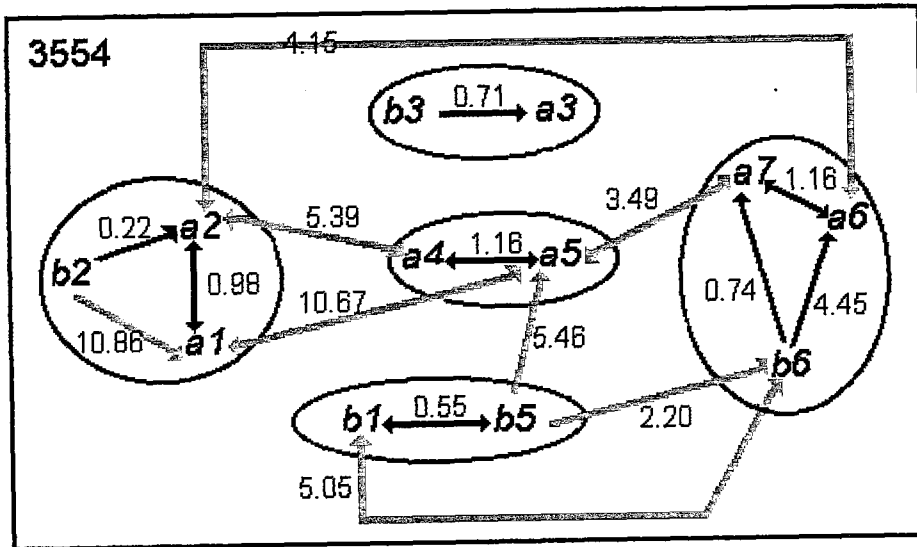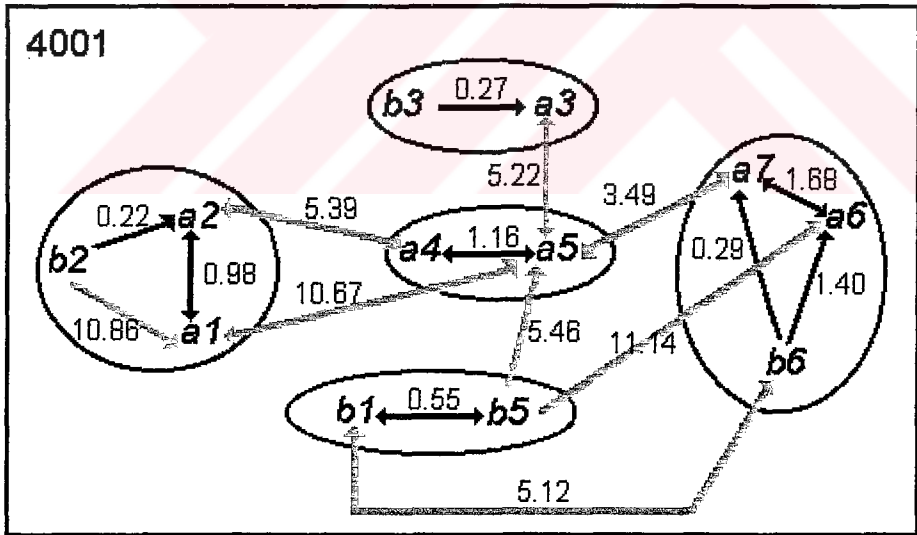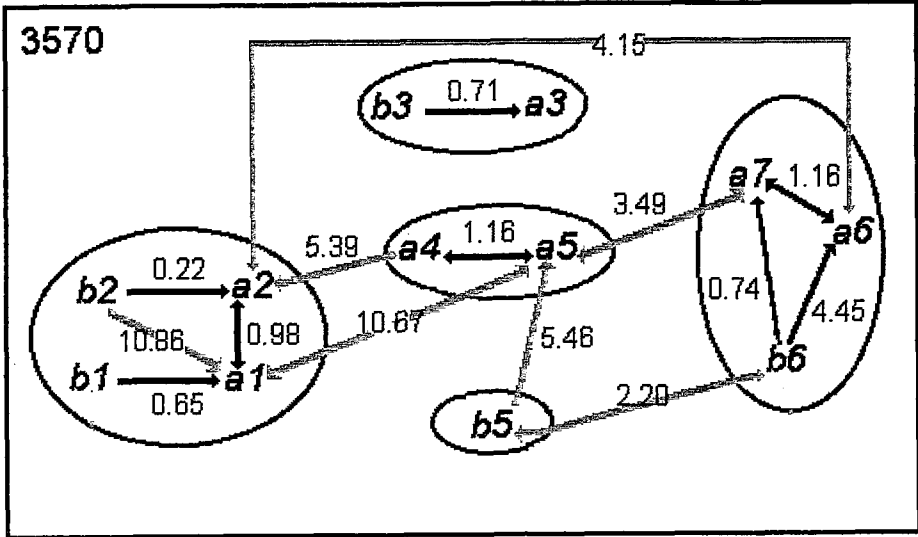Only the pairwise interactions with transfer times less than 12 ps are shown (see Table 3.1 and the text).
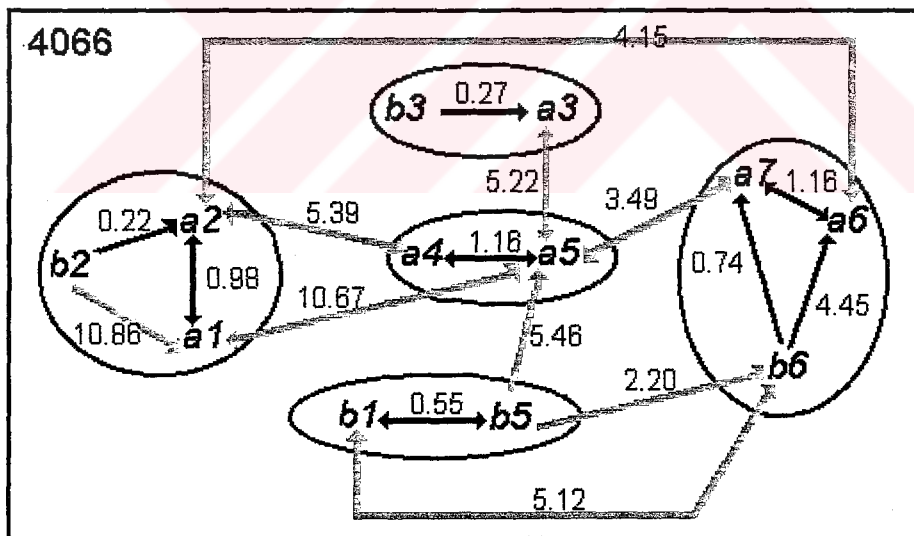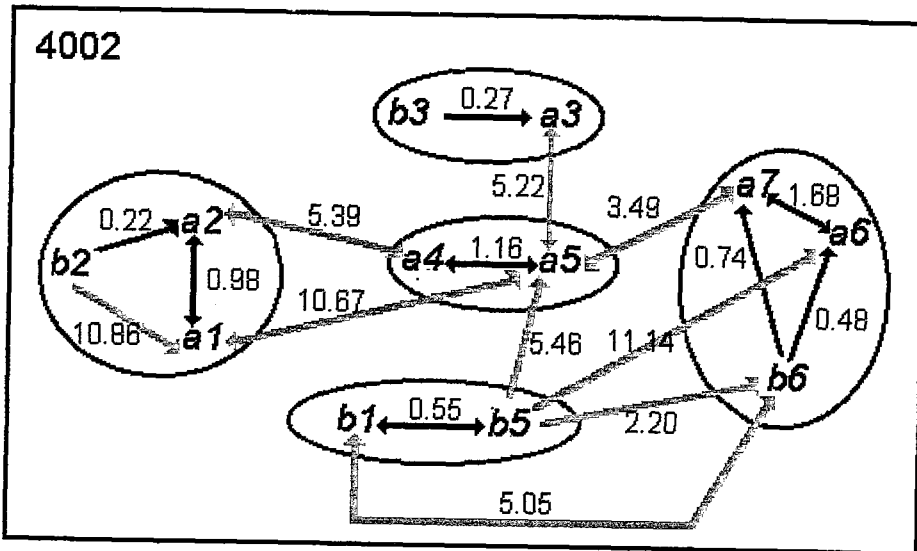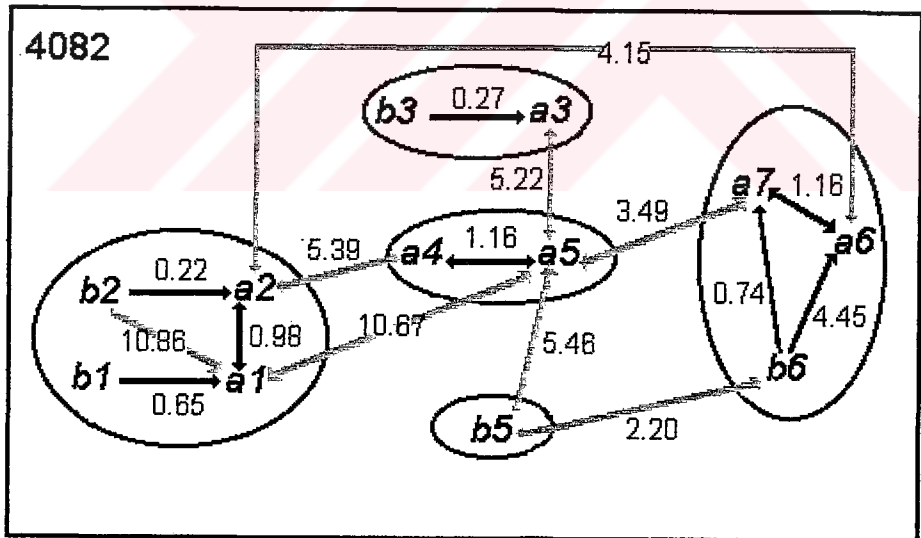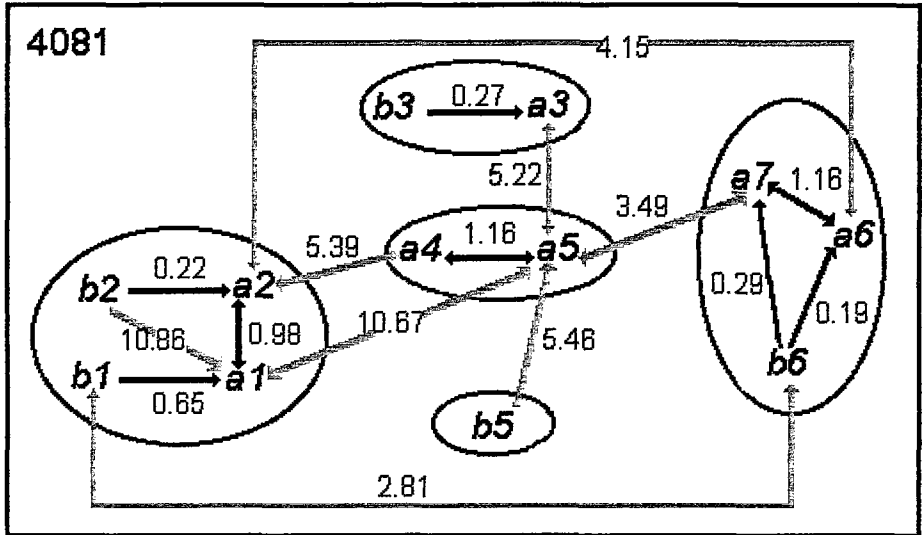
Figure 4.1: (continued).

41

Figure 4.1: (continued).

Figure 4.1: (continued).

Figure 4.1: (continued).

Figure 4.1: (continued).

Chl $b1$ is the key molecule that distinguishes between the two different compartmental classes. The configurations in which Chl $b1=1$ belong to the first class and those with Chl $b1=0$ belong to the second. The distinction between the two groups is due to the differences between the transfer times of two specific Chl pairs: $b1$-$b5$ and $b1$-$a1$. $b1$ to $a1$ transfer is very fast when $b1=0$ (0.65 ps) while it is about 30 times slower when $b1=1$. On the other hand, the equilibration between $b1$ and $b5$ is very fast when $b1=1$ (0.55 ps) and is 40 times slower when $b1=0$.

We first would like to comment on the possible roles of the compartments in the *in vivo* energy transfer pathways in LHCII. LHCII *in vivo* is an aggregated form of the trimeric LHCII. One therefore expects three levels of energy transfers: transfers within a monomer; transfers within a trimer; transfers between trimers. Upon examination of the block diagrams given in Figure 4.1 and the time scales of the intermonomer transfer pathways given in Table 3.2, the probable roles of each of the compartments for these transfers may be suggested. Except in compartment 2 ($a4$-$a5$), there is at least one Chl b molecule at the edge and it either feeds the Chls a of the same compartment or equilibrates with another Chl b in the same compartment. a4-a5 compartment in both of the compartmental structures identified above receives excitation from all the other compartments in the same monomer. The strongest connection of this compartment with compartment 4 is through $a2$-$a4$ interaction. $a5$ also receives from $a1$, but at a much slower rate. The $a3$-$b3$ compartment also has a good interaction with $a5$ if $a3=0$. $b5$ to $a5$ transfer is the main transfer pathway between

compartments 2 and 5. *a5-a7* transfer is the root connecting the *a4-a5* and *a6-b6-a7* compartments. This kind of directionality makes the *a4-a5* compartment the main candidate for the intermonomer transfers. For our configurations, only two of the compartments (*b3-a3* and *a4-a5*) are involved in the intermonomer transfer. The connection of *a5* and *b5* of one monomer to the *a4* of the adjacent one are the strongest intermonomeric transfer pathways. Having the Chl *a* molecules close to the outside boundary of the complex (*a2, a6,* and *a7*) compartments *a1-a2-b1-b2* (or *a1-a2-b2*) and *a6-b6-a7* could be the main exit points to the other trimers.

We now would like to comment on the differences between the origins of the fast, intermediate and slow decay components using our compartmental pictures.

b1 is either slow or intermediate: If *b1*=1, it always contributes to the slow component. In this orientation *b1* is in the same compartment with *b5*. *b1-b5* equilibration is very fast (0.55 ps), however the exit time to another Chl *a* molecule is always slow (around 20 ps). *b1*=1 equilibrates with *b6*= 0 or 1 in about 5 ps. If *b1*=0, it is then in good connection with *a1*. The intracompartmental decay of *b1* scales intermediate. *b1*=0 equilibrates with *b6*=1 within a few picoseconds and the lifetime is slightly shortened.

b2 always contributes to the fast decay component and its decay time is almost fixed: The decay of *b2* is mainly due to *b2-a2* transfer and the decay rate is fixed around 0.220 ps.

Decay of Chl b3 excitation is either fast or intermediate: The main decay route of Chl *b3* is *b3-a3* transfer. The *a3* orientation is not fixed. If *a3*=1, its

only good connection is to *b*3 and the decay scales intermediate (around 0.70 ps). *a*3=0 is open to *a*3-*a*5 transfer in addition to its good connection to *b*3. In this case, *a*3(0)-*a*5(0) transfer (5.22 ps) is much slower than *b*3(1)-*a*3(0) transfer (0.27ps). Therefore the *b*3-*a*3 transfer times in both possibilities appear as the decay times of *b*3 without further reduction.

Chl b5 always contributes to the slow decay component: If *b*5 is in the same compartment with *b*1, the equilibration between the two is very fast. However in both compartmental structures, the major decay channel of *b*5 is its transfer to *a*5. As the *b*5-*a*5 pair has a fixed (1-0) orientation in all of our configurations, Chl *b*5 always contributes to the slow decay component.

Decay of Chl b6 is either fast or intermediate: Being a member of the compartment consisting of *b*6, *a*6, and *a*7, the decay of Chl *b*6 is never slow. In this compartment only *a*7 has a fixed orientation, there are therefore four possible *b*6-*a*6-*a*7 combinations. In all these combinations, at least one of the pairs (*b*6-*a*6 or *b*6-*a*7) is either fast or intermediate. More specifically, *b*6-*a*6-*a*7 triplet is fast (around 0.220-0.250 ps) for the 0-1-0 and 1-1-0 combinations. For the 0-0-0 arrangement *b*6 contributes mostly to the intermediate component (0.425-0.450 ps) and having two fast *b-a* pairs 1-0-0 combination is 'ultrafast ' (around 0.110 ps).

4.B Comparison with the recent experimental results

In this section, we compare our fit results given in Table 4.1 with the recent experimental results summarized in Table 2.1.

The time scales of our fast, intermediate, and slow components are in good agreement with the lifetimes reported in different experiments. The lifetimes of less than 0.3 ps (fast) are observed/deduced by several groups, as well as the lifetimes of around 0.5 to 1 ps (intermediate). The coexistence of two components in the subpicosecond scale is recently reported by Visser et. al. [23]. Different experiments have yielded different lifetimes for the slow component. However, most agree on the existence of a phase with a lifetime of several picoseconds. Pallson et. al. [20] and Visser et. al. [23] agree that the subpicosecond part of the decay is about 80%. Visser and co-workers have furthermore estimated the relative contributions of the fast and the intermediate components to be about equal and around 40 % each. They consequently proposed that of the five Chl b molecules in the monomeric LHCII, two are fast, two are intermediate, and one is slow. Bittner and co-workers data [21,22] are significantly faster than the others and could be interpreted to contain mainly two subpicosecond processes. 65% of the decay is attributed to the fast component.

All the configurations belonging to the compartmental class (b1=1) would be excluded if we compare our results with the Visser/Pallson data. The b1=1 configurations can furthermore be grouped into two in terms of their overall decay behavior. Those with a3=1 display all three distinct decay phases (e.g., 3489, 3490, 3553, and 3554), while the ones with a3=0 (4001, 4002, and 4066) are strongly biphasic. The later group could be interpreted to display the biphasic character reported by Bittner and co-workers. If the

transfer times are about 1.5 times faster (i.e., C'_{ab} =2.5 nm^6/ps), then the agreement could be considered reasonable. The predictions on 3489 is in agreement with Visser [23,29] who has recently analyzed the transfer pathways of this particular configuration in more detail than we have presented here. The configurations of the second compartmental class ($b1=0$) having only one slow Chl b molecule, $b5$, have a much better overall agreement with the Pallson/Visser results.

The origins of the similarities and the differences between the decay characteristics of the selected configurations can be easily understood using our compartmental pictures given in Figure 4.1. It is however rather difficult to narrow down the possibilities further at the current level of experimental information.

4.C Concluding remarks

The b to a excitation energy transfer in LHCII can be described reasonably well with the Förster mechanism within Kühlbrandt and Gülen hypotheses. This means that time scales for b to a energy transfer have been established. A detailed assignment of the energy transfer pathways is provided. The possible roles of each Chl in energy transfer have been identified. An explanation which satisfactorily reproduces the main features

of the femtosecond transient absorption results as well as the measurements in the frequency domain is provided.

We have avoided further conclusions on the basis of the energy transfer processes observed in the Chl *a* spectral region. The spectral properties of the Chl molecules should be more carefully modeled to correlate the data reported for *a-a* transfers [23] with the structure. Our numerical procedures can be easily modified to include spectral details.

Future experimental data with better time and wavelength resolution will no doubt help to differentiate between several configurations. On the basis of the results we have presented, time-resolved measurements on the well-characterized mutants are projected to be more informative than the better-resolved native LHCII data. Since we have clearly identified the possible roles of each Chl molecule in the energy transfer dynamics, we are in a position to make very definite predictions on what to expect if the energy transfer paths are re-engineered. This point will be discussed in the near future in more detail. One can already follow the predictions by viewing our compartmental pictures.

REFERENCES

[1] Barber, J., " *Biophysics of photosynthesis* ", Rep. Prog. Phys., 41, 1157-1199 (1977).

[2] Knox, R.S., " *Excitation energy transfer and migration: theoretical considerations* ", In: Bioenergetics of Photosynthesis (Govindjee, ed.), Academic Press, 183-221 (1975).

[3] Youvan, D.C. and Marrs, B.L.,"*Molecular mechanisms of photosynthesis*", Scientific American, 42-48 (June, 1987).

[4] Hunter, N., " *Molecules of the green machine* ", New Scientist, 60-63 (28 April, 1988).

[5] Fleming, R. and van Grondelle, R., "*The primary steps of photosynthesis*", Physics Today, 47, 48-55 (1994).

[6] Van Grondelle, R., Dekker, J.P., Gillbro, T. and Sundström, V., " *Energy transfer and trapping in photosynthesis* ", Biochim. Biophys. Acta, 1187, 1-65 (1994).

[7] Kühlbrandt, W., Wang, D.N. and Fujiyoshi, Y., " *Atomic model of plant light-harvesting complex by electron crystallography* ", Nature (London), 367, 614-621 (1994).

[8] Gülen, D., van Grondelle, R. and van Amerongen, H., " *Structural information on LHCII as obtained from exciton calculations and polarized spectroscopy* ", In: Photosynthesis: From Light to Biosphere (Mathis, P., ed.), Kluwer Academic Publishers, Vol.1, 335-338 (1995).

[9] Gülen, D., van Grondelle, R. and van Amerongen, H., " *Structural information on the light-harvesting complex II of green plants that can be deciphered from polarized absorption characteristics* ", (submitted to J. Phys. Chem.).

[10] Van Amerongen, H., Kwa, S.L.S., van Bolhuis, B.M. and van Grondelle, R., " *Polarized fluorescence and absorption of macroscopically aligned light harvesting complex II* ", Biophys. J., 67, 837-847 (1994).

[11] Nussberger, S., Dekker, J. P., Kühlbrandt ,W., van Bolhuis, B. M., van Grondelle, R. and Amerongen, H., " *Spectroscopic characterization of three different monomeric forms of the main chlorophyll a/b binding protein from chloroplast membranes* ", Biochemistry, 33, 14775-14783 (1994).

[12] Hemelrijk, P.W., Kwa, S.L.S., van Grondelle, R. and Dekker, J.P., " *Spectroscopic properties of LHCII, the main light - harvesting chlorophyll a/b protein complex from chloroplast membranes* ", Biochim. Biophys. Acta, 1098, 159-166 (1992).

[13] Reddy, N.R.S., van Amerongen H., Kwa, S.L.S., van Grondelle, R. and Small, G.J., " *Low-energy exciton level structure and dynamics in light-harvesting complex II of green plants* ", J. Phys. Chem., 98, 4729-4735 (1994).

[14] Peterman, E.J.G., Dekker, J.P., van Grondelle, R., van Amerongen, H. and Nussberger, S., " *Wavelength-selected polarized fluorescence of monomeric, trimeric, and aggregated light-harvesting complex II of green plants* ", 34, 301-305 (1994).

[15] Krawczyk, S., Krupa, Z. and Maksymiec, W., " *Stark specta of chlorophylls and carotenoids in antenna pigment-proteins LHC-II and CP-II* ", Biochim. Biophys. Acta, 1143, 273-281 (1993).

[16] Lokstein, H., Leupold, D., Voigt, B., Nowak, F., Ehlert, J., Hoffman, P. and Garab, G., " *Nonlinear polarization spectroscopy in the frequency domain of light-harvesting complex II: absorption band substructure and exciton dynamics* ", Biophys. J., 69, 1536-1543 (1995).

[17] Peterman, E.J.G., Hobe, S., Calkoen, F., van Grondelle, R., Paulsen, H. and van Amerongen, H., " *Low-temperature spectroscopy of monomeric and trimeric forms of reconstituted light harvesting chlorophyll a/b complex* ", Biochim. Biophys. Acta, 1273, 171-174 (1996).

[18] Eads, D.D., Castner, E.W., Alberte, R.S., Mets, L. and Fleming, G.R., "*Direct observation of energy transfer in a photosynthetic membrane: chlorophyll b to chlorophyll a transfer in LHC* ", J. Phys. Chem., 93, 8271-8276 (1989).

[19] Du, M., Xie, X., Mets, L. and Fleming, G.R., "*Direct observation of ultrafast energy-transfer processes in light-harvesting complex II* ", J. Phys. Chem., 98, 4736-4741 (1994).

[20] Palsson, L. O., Spangfort, M. D., Gulbinas, V. and Gillbro T., " *Ultrafast chlorophyll b - chlorophyll a excitation energy transfer in the isolated*

light-harvesting complex, LHC, of green plants", FEBS Lett., 339, 134-138 (1994).

[21] Bittner,T., Irrgang, K.D., Renger, G. and Wasielewski, M. R., " *Ultrafast excitation energy and exciton-exciton annihilation processes in isolated light-harvesting complexes of photosystem II (LHC II) from spinach* ", J. Phys. Chem., 98, 11821-11826 (1994).

[22] Bittner, T., Wiederrecht, G. P., Irrgang, K. D., Renger, G. and Wasielewski, M. R., " *Femtosecond transient absorption spectroscopy on the light-harvesting Chl a/b protein complex of photosystem II at room temperature and 12 K* ", Chem. Phys., 194, 311-322 (1995).

[23] Visser, H.M., Kleima, F.J., van Stokkum , I.H.M., van Grondelle, R. and van Amerongen, H., " *Probing the many energy-transfer processes in the photosynthetic light-harvesting complex II at 77 K using energy-selective sub-picosecond transient absorption spectroscopy* ", Chem. Phys., 210, 297-305 (1996).

[24] Van Amerongen, H. and van Grondelle, R., " *Transient absorption spectroscopy in study of processes and dynamics in biology* ", Meth. Enzym., 246, 201-226 (1995).

[25] Knox, R.S., " *Elementary theory of Markoffian excitation transfer processes* ", University of Rochester, Biological Physics Group Technical Report, 13 (1980).

[26] Knox, R.S., "*Theory and modeling of excitation delocalization and trapping* ", In: Encyclopedia of Plant Physiology: Photosynthetic Membranes (Staehelin, L.A. and Arntzen, C.J., ed.), Springer-Verlag

(1985).

[27] Struve, W.S., "*Theory of electronic energy transfer*", In: Anoxygenic Photosynthetic Bacteria (Blankenship, R E., Madigan, M.T. and Bauer, C.E., eds.), Kluwer Academic Publishers, 297-313 (1995).

[28] Förster, Th., "*Zwischenmoleculare energiewanderung and fluoreszenz*", Ann. Physik [6], 2, 55-75 (1948).

[29] Visser, H.M., Ph.D. Thesis, Vrije Univ., Amsterdam, the Netherlands (1996).

[30] Moog, R.S., Kuki, A., Fayer, M.D. and Boxer, S.G., "*Excitation transport and trapping in a synthetic chlorophyllide substituted hemoglobin : orientation of the chlorophyll S_1 transition dipole*", Biochemistry, 23, 1564-1571 (1984).

[31] Shipman, L.L. and Hausman, D.L., "*Förster transfer rates for chlorophyll a*", Photochem. Photobio., 29, 1163-1167 (1979).

[32] Jean, J.M., Chan, C.K. and Fleming, G.R., "*Electronic energy transfer in photosynthetic bacterial reaction centers*", Israel J. of Chem. , 28, 169-175 (1988).

[33] Sauer, K., Smith, J.R.L. and Schultz, A.J., "*Dimerization of chlorophyll a, chlorophyll b and bacterial chlorophyll in solution*", J. Am. Chem. Soc., 88, 2681-2688 (1966).

[34] Kiraly, A.P., "*Excitation energy flow through light-harvesting chlorophyll proteins*", University of Rochester, Biological Physics Group Technical Report, 147 (1995).

APPENDIX

NUMERICAL CONSIDERATIONS

In this appendix, a flowchart of the calculations has been given.

Selection of a configuration

↓

Atomic coordinates

↓

The distances between the Chl pairs, R_{AD}

Orientational factors
$\kappa_{AD}^2 = [\hat{\mu}_A \cdot \hat{\mu}_D - 3(\hat{\mu}_A \cdot \hat{R}_{AD})(\hat{\mu}_D \cdot \hat{R}_{AD})]^2$

Overlap integrals: $C'_{aa} = 5$, $C'_{bb} = 2.5$, $C'_{ab} = 1.67$ nm^6/ps

↓

FÖRSTER RATES ARE ESTIMATED.
$F_{AD} = C'_{AD} \, \kappa_{AD}^2 \, R_{AD}^{-6}$

↓

W ENERGY MATRIX IS FORMED.
$dP(t) = -WP(t)$

↓

PME IS SOLVED (Matlab, EXPM).
Chl *b* DECAY IS SIMULATED.

↓

DECAY IS FITTED TO A SUM OF 3-EXPONENTIALS (Matlab, FUNFIT).

↓

Fit results vs. fs exp. results.

↓

ENERGY TRANSFER PATHWAYS BETWEEN THE CHL MOLECULES ARE IDENTIFIED.